arXiv:0711.0728v1 [hep-ex] 5 Nov 2007

A first measurement of the interaction cross section of the tau neutrino

K. Kodama[1], N. Ushida[1], C. Andreopoulos[2], N. Saoulidou[2,a], G. Tzanakos[2], P. Yager[3], B. Baller[4], D. Boehnlein[4], W. Freeman[4], B. Lundberg[4], J. Morfin[4], R. Rameika[4], S.H. Chung[5], J.S. Song[5], C.S. Yoon[5], P. Berghaus[6], M. Kubantsev[6], N.W. Reay[6], R. Sidwell[6], N. Stanton[6], S. Yoshida[6], S. Aoki[7], T. Hara[7], J.T. Rhee[8], D. Ciampa[9], C. Erickson[9], M. Graham[9], E. Maher[9,b], K. Heller[9], R. Rusack[9], R. Schwienhorst[9], J. Sielaff[9], J. Trammell[9], J. Wilcox[9], T. Furukawa[10], K. Hoshino[10], H. Jiko[10], M. Komatsu[10], M. Nakamura[10], T. Nakano[10], K. Niwa[10], N. Nonaka[10], K. Okada[10], B. D. Park[10], O. Sato[10], S. Takahashi[10], V. Paolone[11], C. Rosenfeld[12], A. Kulik[11,12], T. Kafka[13], W. Oliver[13], T. Patzak[13,c], J. Schneps[13]

(The DONuT Collaboration)

[1]*Aichi University of Education, Kariya, Japan*
[2]*University of Athens, Athens 15771, Greece*
[3]*University of California/Davis, Davis, California 95616, USA*
[4]*Fermilab, Batavia IL 60510, USA*
[5]*Gyeongsang University, Chiju, South Korea*
[6]*Kansas State University, Manhattan, Kansas 66506, USA*
[7]*Kobe University, Kobe, Japan*
[8]*Kon-kuk University, Seoul, S. Korea*
[9]*University of Minnesota, Minneapolis, MN 55455, USA*
[10]*Nagoya University, Nagoya 464-8602, Japan*
[11]*University of Pittsburgh, Pittsburgh, PA 15260, USA*
[12]*University of South Carolina, Columbia, South Carolina 29208, USA*
[13]*Tufts University, Medford, MA 02155, USA*

[a]Presently at Fermilab
[b]Presently at the Massachusetts College of Liberal Arts, North Adams, MA 01247, USA
[c]Presently at the Université Paris 7, Paris, France

The DONuT experiment collected data in 1997 and published first results in 2000 based on four observed ν_τ charged-current (CC) interactions. The final analysis of the data collected in the experiment is presented in this paper, based on 3.6×10^{17} protons on target using the 800 GeV Tevatron beam at Fermilab. The number of observed ν_τ CC interactions is 9, from a total of 578 observed neutrino interactions. We calculated the energy-independent part of the tau-neutrino CC cross section ($\nu + \bar{\nu}$), relative to the well-known ν_e and ν_μ cross sections. The ratio $\sigma(\nu_\tau)/\sigma(\nu_{e,\mu})$ was found to be $1.37 \pm 0.35 \pm 0.77$. The ν_τ CC cross section was found to be $0.72 \pm 0.24 \pm 0.36 \times 10^{-38}$ cm^{2}GeV^{-1}. Both results are in agreement with expectations from the Standard Model.

PACS numbers: 14.60.Lm, 13.25.Ft, 13.35.Dx, 02.50.Sk

February 11, 2013

I. INTRODUCTION

The tau neutrino, ν_τ, was assigned its place in the Standard Model after its electrically charged weak isospin-$\frac{1}{2}$ partner, the τ lepton, was discovered in 1975 [1]. The observation of identifiable ν_τ interactions, in a manner similar to ν_e [2] and ν_μ [3] interactions, did not immediately follow. The difficulty of measuring ν_τ interactions was due to the relative scarcity of the sources of ν_τ and the lack of sufficiently powerful detection methods to unambiguously identify the short-lived τ lepton (mean lifetime 2.9×10^{-13} s) produced in ν_τ charged-current interactions. These challenges were overcome in the observation of four ν_τ interactions by the DONuT (**D**irect **O**bservation of **Nu**-**T**au) collaboration, in 2000 [4][5], twenty-five years after the τ was discovered. Analysis of our full data set yielded nearly three times as many neutrino interactions of all flavors as reported in Ref. [4]. This paper reports our final results, bringing the DONuT experiment to a completion.

The purpose of the DONuT experiment was to study ν_τ charged-current (CC) events,

$$\nu_\tau + N \to \tau^- + X, \tag{1a}$$
$$\bar{\nu}_\tau + N \to \tau^+ + X. \tag{1b}$$

However, during data taking, DONuT was recording interactions of neutrinos of all flavors: ν_e CC events

$$\nu_e + N \to e^- + X, \tag{2}$$

ν_μ CC events

$$\nu_\mu + N \to \mu^- + X, \tag{3}$$

and neutral-current (NC) events

$$\nu_\ell + N \to \nu_\ell + X, \quad \ell = e, \mu, \tau \tag{4}$$

and analogously for the antineutrinos.

Reaction (1) must be distinguished from charm production in reactions (2) and (3), since the tau-lepton and the charmed particles have comparable lifetimes and decay signatures:

$$\nu_\ell + N \to \ell^- + C^\pm + X, \quad \ell = e, \mu \tag{5}$$

where $C =$ D, D$_s$, or Λ_c. Another background considered here were secondary hadron ineractions in NC neutrino events, reaction (4),

$$\begin{aligned} \nu_\ell + N \to \ \ & \nu_\ell + h^\pm + X, \quad \ell = e, \mu, \tau, \\ \text{followed by} \quad & h^\pm + N \to (1 \text{ or } 3 \text{ prongs}) + X^0 \end{aligned} \tag{6}$$

The experimental apparatus and techniques, have been described in detail elsewhere [6][7]and are only summarized here.

The location of vertices in the emulsion data, tagging leptons and the subsequent search for secondary vertices, were accomplished with high efficiency. This allowed a detailed event-by-event analysis with small and calculable background levels. Further, the large amount of information in the emulsion/spectrometer system permitted the use of powerful multivariate methods yielding probabilities for each candidate event to be signal or background. The measured ν_τ cross section was computed using the final sample of all ν_τ, ν_e, and ν_μ interactions located in the emulsion.

The organization of this paper is as follows. First we give an overview of the neutrino beam and detector elements. Next, there is a synopsis of triggering and filtering that produced the interaction sample. We then give important details of the emulsion detector. The analysis is reviewed by outlining the lepton identification procedures, the Monte Carlo, event location in the emulsion and secondary vertex search. After a survey of the entire data set including neutrino interactions of all flavors, the ν_τ cross section analysis is described, systematic error sources are discussed, and the results are presented.

II. NEUTRINO BEAM AND DETECTOR

Primary beam. The number of 800-GeV protons that struck the beamdump was measured by devices that integrate charge collected from secondary emission from a foil. These monitors were calibrated with a beta source before the experiment began. Several times during the course of the run, these devices were calibrated against coil pickups and other monitors installed in the accelerator extraction complex. These checks showed that the primary beam monitors were consistent within 5% at intensities of 5×10^{12} to 1×10^{13} protons per spill. Losses in the beamline were small ($\approx 10^{-5}$), and no other corrections were applied. The monitors' output was digitized and recorded at the experiment, and gated by the trigger electronics. A total of 3.54×10^{17} protons were recorded during the live-time of the experiment. A systematic uncertainty of 5% was assigned to the value of the total number of protons in the beamdump.

DONuT beamline. The 800-GeV protons from the Tevatron were stopped in a beamdump in the form of a solid block of tungsten alloy. The typical intensity was 8×10^{12} protons for 20 seconds each minute, or about 20 kW of beam power. Immediately following the beamdump were two dipole magnets with solid steel poles, providing both absorption of interaction products and deflection of high-energy muons away from the beam center. Following the magnets was an additional 18 m of passive steel shielding limited to within 2 m of the beamline. Emerging at the end of this shield, 36 m from the beamdump, were neutrinos and muons. The muons were mostly contained in horizontal fan-like distributions on each side of the centerline. The neutrino beam design is shown in Fig. 1.

Neutrino beam. Neutrinos in the DONuT beam originated from decays of particles within the hadron shower created by a primary proton interaction. Neutrinos from decays of charmed particles are called *prompt* neutrinos, and neutrinos from decays of $\pi^{\pm}$ and $K^{\pm}$ are called *non-prompt* neutrinos. About 97 % of the neutrino flux from the beamdump was composed of ν_e and ν_μ, the rest being ν_τ. 93% of the ν_e's were prompt, while ν_μ's had substantial components of both prompt and non-prompt neutrinos. All ν_τ's were prompt. Most of them originated in leptonic decays of D_s mesons. The decay mode $D_s \to \nu_\tau \tau$ yielded two tau neutrinos within a distance of a few millimeters. This decay length is much less than the interaction length of six centimeters. The calculated neutrino energy spectra of all the neutrinos that interacted in the DONuT target are shown in Fig. 2.

Emulsion target. The target - schematically depicted in Fig. 3 - was the core of DONuT. Its capabilities and performance were matched to the task of recognizing neutrino interactions containing tau leptons. The main component of the target assembly was 250 kg of nuclear emulsion stacked in modular fashion along the beamline. A total of seven emulsion modules in the target station were exposed, with a maximum of four modules in place at any time during the experiment.

Each module was exposed for a limited time to avoid track density higher than 10^5 tracks per cm^2 that would make the emulsion data analysis inefficient. To further assist the analysis, single *Changeable Sheets* were mounted 1 cm downstream of each emulsion target module and replaced ten times more often.

Scintillating fiber tracker (SFT). Integrated into the emulsion target station were 44 planes of the SFT built using 0.5-mm-diameter scintillating fibers to provide medium-resolution tracking and a time-stamp for each event.

Spectrometer. The emulsion target station was followed by a spectrometer consisting of a large-aperture dipole magnet and up to six *drift chambers*. A lead- and scintillating-glass *electromagnetic calorimeter* aided in identifying electrons and measuring their energy. Behind the calorimeter, muons were tagged with a *Muon-ID* system consisting of three steel walls each followed by two crossed proportional-tube planes. The plan of the spectrometer is shown in Fig. 5.

III. SPECTROMETER DATA COLLECTION AND REDUCTION

A. Triggering and data acquisition

Trigger. A trigger for recording neutrino interactions required that no charged particles entered the emulsion from upstream and at least one charged particle emerged from an emulsion target. The scintillation-counter triggering system included a veto wall upstream of the emulsion target and three hodoscope planes distributed between and downstream of the emulsion modules, shown in Fig. 3. The average trigger rate was 5.0 Hz, with a livetime of 0.89. The trigger efficiency was calculated using simulated neutrino interactions and measured efficiencies for all counters. The efficiency for triggering on ν_e CC, ν_μ CC, ν_τ CC, and NC interactions was 0.98, 0.96, 0.96, and 0.86, respectively. Detailed description of the triggering system can be found in Ref. [7].

Data acquisition. The architecture of the data aquisition was based on the Fermilab DART product [8], using VME-based microprocessors to control the transport of data from the VME buffers to a host computer. The host computer served as both the data monitor and as the data logger to tape (Exabyte 3500). The average event size was 100 kB, with a throughput of 10 MB per beam cycle of one minute.

B. Filtering and scanning

A total of 6.6×10^6 triggers from 3.54×10^{17} protons on target were recorded. In this data set, only about 10^3 neutrino interactions were expected. This implied that the great majority of the triggers were background processes satisfying the simple trigger requirements of Section III A. Data from the electronic detectors were used to extract the neutrino interaction candidates in a two-step process.

Software filter. The time difference between any two trigger counter signals was required to be within 2.5 ns. Data from the SFT and from the drift chambers were then used to reconstruct tracks and to search for a vertex near one of the emulsion targets. Triggers that did not yield a candidate vertex were eliminated. This software filter reduced the number of recorded triggers by a factor of 300. Efficiencies for keeping neutrino interactions were determined by Monte Carlo studies to be 0.98 (for CC events) and 0.96 (for NC events).

Physicist scan. In the second step, the remaining triggers were scanned individually by a physicist using a graphical display. This step rejected events originating from particle showers produced by high-energy muons and checked for errors in reconstruction and other pathologies. Most of the events were rejected quickly and with high confidence. This visual scanning reduced the data by another factor of 20, yielding 866 neutrino interaction candidates within one of the emulsion modules which had a visible energy over 2 GeV. The efficiency of the physicist scan was found to be (0.86 ± 0.07).

The estimated total efficiency for retaining a ν_τ CC interaction with the electronic detectors was 0.72 after triggering, filtering and scanning. For ν_e (ν_μ) CC interactions these efficiencies were 0.73 (0.71), and for NC interactions it was 0.64.

C. Neutrino event sample

The resulting sample included 866 events that were likely neutrino interactions of all flavors with the vertex located within the fiducial volume in the emulsion target.

We report here on the analysis of all the events for which the neutrino interaction vertex was found in the emulsion, referred to thoughout as *located events*. Although locating the vertex in the emulsion was attempted for each of the 866 events, only 578 events were located, as described in Section VII.

Events in the initial sample that were not located in the emulsion were not used in the analysis described below.

IV. THE EMULSION

The DONuT emulsion modules were the first modern implementation of a design that interleaves metallic sheets (stainless steel) with emulsion sheets to achieve high mass to increase the number interactions and high precision for tau recognition. As illustrated in Fig. 4, two designs of these 'Emulsion Cloud Chambers' were used in DONuT: both used 1-mm thick steel sheets interleaved with emulsion sheets having 100 μm thick emulsion layers on both sides of a plastic base. The designs differed in thickness of the base, one was 200 μm and the other 800 μm thick. The third design had 350 μm thick emulsion layers on 90 μm thick base. More details about the emulsion target design can be found in Ref. [6].

After exposure, the emulsion target modules were transported to Nagoya University in Japan, where they were disassembled and individual emulsion sheets developed. The Changeable Sheets were developed at Fermilab.

The information from a small emulsion volume surrounding the interaction point predicted by the spectrometer data was fully digitized and used in a manner similar to the information from an electronic detector. The size of the volume needed to be large enough to contain the vertex but small enough to be compatible with the capabilities of the emulsion scanning machines.

Once the desired emulsion volume was determined, the individual emulsion sheets were digitized using automatic scanning and digitizing apparatus at Nagoya University. The Nagoya group developed this technology over the years, starting in 1974. The DONuT emulsion data were obtained using Ultra Track Selector (UTS) digitizers [9] with scanning rate of 1 cm^2/hour, a factor of five improvement over the technology used to obtain the first DONuT results of Ref. [4] allowing for greatly increased location efficiency.

Emulsion data. The UTS automated scanning stations found and digitized track segments ("microtracks") in the emulsion layers on both sides of the transparent plastic base. Both the position and angle of each segment were computed and recorded in real time. Efficiency for detecting microtracks was measured to be greater than 0.97.

Complete tracks were built layer by layer. Each microtrack was examined to see if it had a connectable microtrack in adjacent emulsion layers. Once reconstructed, the tracks were added to a data set unique to the given scan volume.

An important tool used in the offline emulsion data processing were high-energy muons from the beamdump that penetrated the shielding and were recorded in the scanned emulsion volume as through-going tracks with little measurable scattering, called "calibration tracks" below.

Data quality checks. A systematic methodology was developed to quantify the quality of tracks found in digitized emulsion images. Two quantities were used: (a) position accuracy σ as measured by rms displacement of microtracks from fitted calibration tracks, and (b) emulsion read-out efficiency ε, representing the fraction of identified calibration-track microtracks actually seen in any one emulsion plate. Emulsion data passed the data quality check when $\sigma \leq 1.0\,\mu$m, and $\varepsilon \geq 0.9$. Reasons for poor data quality could be a damaged emulsion (lost forever), difficulty in emulsion digitization (to be re-digitized), or a systematic problem such as emulsion-sheet slipping within a stack which can be corrected as detailed below. More than 50% of events where the predicted vertex was not initially found in the emulsion fell into the poor-data-quality category.

Emulsion-sheet slipping: Occasionally, emulsion sheets slipped one with respect to another during exposure. An alignment method was therefore devised to correct for it using the calibration tracks. The alignment parameters of interest included the distance between the emulsion layers, the relative shifts in transverse direction and the shrinkage of the emulsion layers. Alignment between adjacent sheets was determined within 0.2 μm.

V. PARTICLE IDENTIFICATION

A. Muons

A muon tag was assigned to a track if there were at least four hits in the six proportional-tube planes of the muon-ID system. The per-tube efficiency for muons was measured to be 0.96, and the geometrical acceptance of the muon ID system was estimated by Monte Carlo to be 0.76, yielding an overall efficiency of 0.73. The muon spectra are shown in Fig. 6.

Muon track momentum could be measured in one of two very different ways: *(i)* from the curvature in the spectrometer, and *(ii)* from multiple coulomb scattering (MCS) in the emulsion.

Spectrometer measurement. In the spectrometer, track momentum was measured using a 4 T magnet with $\int Bdl = 0.75$ T m. For muons, $\Delta p/p$ was 11% for momentum p of 20 GeV/c, increasing to 100% at $p = 250$ GeV/c.

Emulsion measurement. The high spatial precision of the tracking in emulsion, in conjunction with an adequate sampling rate, allowed the calculation of track momentum from the visible scattering of the track's segments (microtracks) in individual emulsion plates.

A special emulsion track scan was performed on all tracks found in candidate neutrino events for the dual purpose of the multiple coulomb scattering measurement and electron identification (see Section V B 1 below). Momentum was successfully measured using multiple coulomb scattering for 64% of the tracks in the sample.

The method was validated by test-beam experiments which showed that the beam momentum of 0.8 and 1.5 GeV/c (4 Gev/c) could be measured by the emulsion with a resolution of 23% (30%) [10] ([6]). A comparison of track momenta measured with both the emulsion and spectrometer is shown in Fig. 10.

The upper limit of the momentum measured this way was determined by the number of samples, the angle of the track, the quality of the emulsion data and the type of emulsion module. A typical upper limit was 25 GeV/c.

B. Electrons

1. *Electron identification*

The electron analysis was less straightforward since it involved several systems. Since the emulsion modules were two to three radiation lengths thick, most events containing electrons would exhibit showers in the SFT and in the electromagnetic calorimeter. These two electronic detectors were used to find the most likely initial energy of the electron from an algorithm using both energy (pulse height) and geometrical shower development.

A special *electron ID scan* was performed on all emulsion tracks. This scan followed each track from the vertex to the most downstream plate. An area of 600 μm $\times$ 600 μm centered on the track was digitized in each emulsion plate. Electrons were identified by electron-positron pairs found within 20 μm of the track. The electron-ID scan was most effective for vertices located in the upstream part of an emulsion module.

The efficiency for electron tagging using the spectrometer was estimated to be 0.80 ± 0.04. The electron tagging efficiency using emulsion data varied with path length, with a maximum of 0.86 for tracks passing through at least 2 X_0. The integrated efficiency of identifying an electron in the emulsion was 0.66.

The total electron identification efficiency as a function of energy is shown in Fig. 7.

2. Electron energy measurement

The target/fiber system was also used to estimate the electron (or gamma) energy. Since the scintillating fiber system response was calibrated to minimum ionizing particles, the total pulse height in a shower could be summed for each station providing a direct measure of energy. The energy estimates at each station were input variables for an algorithm to compute electron energy from shower development. The calorimeter information was added for showers that penetrated less than six radiation lengths of emulsion (approximate shower maximum). The estimated energy resolution, $\Delta E/E$, was 30%.

Since the beamline could not be configured for transport of electrons, electron identification and energy estimate relied heavily on Monte Carlo simulation. A selection of probable electrons from interactions in the most downstream emulsion-target module, analyzed for momentum in the spectrometer and energy in the calorimeter, showed that the calorimeter calibration was consistent with a calibration method using muons as minimum ionizing particles.

VI. MONTE CARLO SIMULATION

The production of neutrinos in the beamdump, their transport through the shielding system, and their interactions in the emulsion target were simulated with a GEANT3-based Monte Carlo software. The emulsion target and all electronic detectors in the spectrometer were simulated, taking into account their measured efficiencies and other response characteristics peculiar to each system.

The production of charmed particles by 800 GeV protons in the beamdump were generated using a phenomenological formula,

$$\frac{d^2\sigma}{dx_F dp_T^2} = A\, e^{-bp_T^2}\, (1 - |x_F|)^n \tag{7}$$

where x_F is Feynman x and p_T is transverse momentum. The values of b and n in Eq. (7) depend on the charm species. The details of the simulation of neutrino production in the beamdump via charm particle decays are given in Appendix A. If the path of a neutrino originating from a charm decay intersected the emulsion target, a deep-inelastic neutrino-nucleon interaction was generated using LEPTO v6.3.

The simulated particles from the interaction were recorded in each detector and "digitized" as appropriate for electronics used in the experiment. This Monte Carlo data was stored in the format used by the data acquisition system and was analyzed in the same manner as experimental data. In addition, a separate file was generated with data from the charged particles within the emulsion sheets. The data contains microtracks in each emulsion layer, but it does not directly simulate the algorithms used in the UTS emulsion digitizers.

The Monte Carlo was the primary tool for computing acceptance of the neutrino flux in the emulsion target needed for the cross section analysis. It was also used to establish selection cuts, develop electron identification algorithms, and probe systematic effects from charm particle production uncertainties.

VII. EVENT LOCATION IN THE EMULSION

Two methods were used by DONuT to locate neutrino inetraction vertices in the emulsion target, both starting with extrapolation of spectrometer tracks back to the emulsion target. The SFT was the principal device for making the initial vertex prediction.

A. Event location by Netscan

Netscan event location was a multi-step process. Initially, information from the electronic detectors was used to fit charged-particle tracks, and reconstruct a neutrino-interaction vertex whenever possible. The resolution of these detectors enabled vertex predictions with a precision of about 1 mm transverse and 5 mm along the neutrino beam direction. Next, both the position and size of the scanning volume were determined using the spectrometer prediction, and all microtracks within the scanning volume were digitized.

After the necessary alignment of the emulsion data, track pairs were examined to see if they formed a vertex. The following selection criteria were applied:

- Tracks must start within the volume and cannot be connected to any aligned microtracks in two adjacent upstream emulsion layers to reject penetrating muon tracks.
- Tracks must be constructed from at least three microtracks and have a good χ^2 fit. These requirements reduce the number of low momentum tracks.
- The remaining tracks were tested for vertex topology. Tracks were associated when the impact parameter at the best vertex position was less than 5 μm.

Out of the total of $\sim 10^4 - 10^5$ microtracks per $5 \times 5 \times 15$ mm^3 emulsion volume, only a few vertex candidates remained after the three requirements were imposed. To confirm a vertex candidate, (*i*) the emulsion plates near the vertex point were examined by a physicist using a manually controlled microscope to check for consistency of the neutrino interaction hypothesis (i.e. neutral particle interaction), and (*ii*) the emulsion track information was compared with the hits in the SFT to verify that all tracks were associated with the same event. For interaction vertices that passed all the checks, all tracks in the event were refit using the emulsion information.

B. Event location by Backscan using Changeable Sheets

The Changeable Sheets were used when the vertex prediction was problematic: the event was either too complex to have an accurate vertex prediction made, or, on the other hand, only one charged track was reconstructed in the SFT, so that the interaction point was constrained only in the two transverse dimensions. In this case, the SFT track was extrapolated to the CS position and the emulsion data in this sheet was searched for a track matching both position and angle. If found, the track could be followed into the emulsion target module with much greater accuracy to greatly reduce ambiguity in high track-density regions. The SFT-CS matched tracks were followed upstream, through the sheets of the target module, using emulsion scanning within a cylindrical volume (used in Ref. [4]) or within a conical volume with transverse dimensions increasing along the track, used in this analysis. The latter scan resulted in much larger emulsion volume being scanned to increase event location efficiency, but also greatly increased the digitizer work load. This was only possible when UTS digitizers became available.

If a track penetrated all the way to the most upstream sheet, the track was rejected. If the track was found to be missing in upstream sheets, it was assumed to originate in the space between emulsion layers. All tracks followed in this way were checked to ensure that they did not originate as an e^+e^- pair, a secondary interaction or as an emulsion inefficiency causing a gap in a throughgoing track. If these background hypotheses were rejected, the track was assumed to originate from a primary vertex of a neutrino interaction. All other emulsion tracks that passed within 5 μm of this track's endpoint were checked to see if they were likely to originate in the same interaction.

C. Special cases

Special methods were developed for events with large number of hits in SFT, for which the total pulse height exceeded the equivalent of 650 minium ionizing tracks and no 3-D tracks could be reconstructed. These large-pulse height events are called *LP events* below.

In the *modified CS scan*, a large area (> 1 cm^2) was scanned in the CS nearest to the upstream end of a large SFT shower, and electron signature was searched for in the form of clustered parallel microtracks. If found, the electron was followed by backscan to the vertex. Alternatively, a line was drawn through the shower core in the SFT to better pinpoint the CS area to be scanned, with a typical size of 5×5 mm^2. In this case, no electron signature was required, and all tracks matching the line in position and angle were followed back.

In the *modified Netscan*, a number of lines were drawn in u- and v-projection and extrapolated into the emulsion module. If a candidate vertex region was found, Netscan was applied over an oversized volume, typically $13 \times 13 \times 20$ mm^3.

The two methods yielded similar numbers of events, with a total of 58 LP events located in the emulsion, of which 31 were ν_e events, 9 ν_μ events, 2 ν_τ events and 16 NC events.

D. Location efficiency

The overall efficiency for locating the primary vertex in the emulsion was given directly as the ratio of the number events found and the number of events tried. This ratio is 578/866 or 0.667 ± 0.036.

We note that each module corresponded to 2.5 to 3 radiation lengths and 0.2 interaction lengths, so secondary interactions were a common occurrence. Resulting large hadron/electromagnetic showers hampered track reconstruction and vertex location. There were 188 events classified as LP events, or 22% of the total of 866. A total of 58 LP events were located in the emulsion, representing a location efficiency of 0.31 ± 0.05, to be compared to 0.77 ± 0.04 location efficiency for the regular events (520 located out of a total of 678).

We investigated the located-event sample for possible biases. Fig. 8 displays the distance along the beam direction between the vertex and the downstream edge of an emulsion module, for all 7 modules. The distribution is consistent with being independent of z, with χ^2/ndf to a straight line of 1.7. The vertex distribution in the transverse plane (not shown) is uniform, as expected. The located-event charged multiplicity distribution is compared with expectation in Fig. 9. We conclude that the benefit of using a combination of different location methods was to have uniform location efficiency.

VIII. SECONDARY VERTEX ANALYSIS

A. Decay search criteria

For the located events, the emulsion was digitized again in a smaller volume containing the vertex and optimized for the decay search, typically 2.5mm × 2.5mm × 12mm. The track reconstruction algorithm was the same as that used for vertex location. The decay search was divided into two categories distinguished by topology:

1. *Long-decay search:* Decays in which the candidate parent track passed through at least one emulsion layer.

2. *Short-decay search:* Decays in which only the daughter track was recorded in emulsion.

The strategy was common for both decay topologies under consideration. Once a secondary vertex was found, the event was classified as a one-prong decay, unless additional tracks were found to be associated with the same secondary vertex constituting a three-prong decay.

Tau and charm decays were obtained from the data in a two-step process: *(i)* finding secondary vertices in emulsion data using geometrical cuts, described in this Section, and *(ii)* subsequently imposing topological and kinematical cuts to isolate the signal from the background, described in Section VIII B.

1. *Long-decay search*

The Long-decay search for one-prong decays imposed the following criteria:

- The parent track had one or more microtracks, and a daughter track had three or more microtracks.
- The parent track length: $L_{dec} < 10$ mm.
- The impact parameter b_p of the parent track with respect to the primary vertex: (i) $b_p < 5$ μm if there were at least two microtracks, or (ii) $b_p < (5+0.01\times\delta z)$ μm if there was one microtrack, where δz is the distance from the parent microtrack to the vertex.
- The minimum distance, d_{min}, between extrapolated parent and daughter tracks: (i) $d_{min} < 5$ μm if there were at least two parent microtracks, or (ii) $d_{min} < (5 + 0.01 \times \delta z)$ μm if there was only one parent microtrack.
- (i) The angle between the daughter and parent tracks: $\alpha > 4$ times the angular measurement error, or (ii) The impact parameter b_d of the daughter with respect to the primary vertex: $b_d >$ 4 times the error in the position.

Candidate tracks passing the above criteria were checked in the emulsion by a physicist using a microscope to ensure that (i) the daughter track could not be associated with emulsion tracks upstream of the vertex, (ii) that it was not a part of a e^+e^- pair, and (iii) that there were no alignment problems.

2. *Short-decay search*

The Short-decay search for one-prong decays required the following criteria:

- The daughter track had at least three microtracks.
- The daughter-track impact parameter (IP) with respect to the primary vertex: $b_d < 200$ μm.
- The daughter-track IP w.r.t. the primary vertex: $b_d > 4 \times \sigma_{IP}$, where σ_{IP} is the error on the impact parameter.

Each candidate daughter track was checked visually to insure that it could not be connected to microtracks upstream of the vertex.

B. Tau and charm recognition

To extract the ν_τ signal from events passing the secondary-vertex selection, a set of topological and kinematical criteria was first applied as described in Section VIII B 1 below. In the second step, the amount of signal and background was determined using a multivariate technique featured in Section VIII B 2.

1. Topology and kinematical cuts

ν_τ event topology. The ν_τ CC interactions, reaction (1), produce a τ lepton that typically decays within 2 mm of its origin. Thus, the topological signature for ν_τ events is a track from the primary vertex that gives a secondary vertex at a short distance consistent with the kinematics of the decay. There must be no other lepton from the primary vertex. The topological signature of charm production in reaction (5) is very similar to ν_τ events. Tau and charm events were distinguished primarily by presence of an electron or muon at the interaction vertex. Thus, a ν_e or a ν_μ CC interaction together with a failure in lepton identification constitutes the primary background to the tau sample. The second background considered here were interactions of hadrons produced in neutrino NC interactions, reaction (6), that appeared in the emulsion with a topology of a one-prong or three-prong interaction (or decay).

Kinematical cuts. The following set of criteria were derived from Monte Carlo studies to efficiently extract the ν_τ signal with minimal background. It is a modified version of the selection criteria of Ref. [4]. Long one-prong and trident decays were accepted when the following conditions were satisfied:

- Parent-track angle w.r.t. neutrino direction: $\theta_p < 0.2$ rad.
- Daughter-track angle w.r.t. parent direction: $\theta_d < 0.3$ rad.
- Kink angle: $\alpha < 0.25$ rad.
- Daughter-track IP: $b_d < 500$ μm.
- Transverse momentum of the daughter w.r.t. parent track: $p_T > 250$ MeV/c for hadrons, and $p_T > 100$ MeV/c for electrons and muons.
- Daughter momentum: $p_d > 1$ GeV/c.

Events passing these criteria that did not have an identified electron or muon track from the primary interaction vertex were selected as ν_τ candidate events. In the case of trident secondary vertices, at least one of the secondary tracks must pass all of the above requirements. Fig. 11 shows the distribution of number of kinks versus transverse momentum, p_T, of the daughter w.r.t the parent track, for all tracks satisfying the above criteria *except* the transverse momentum cut. One can see that p_T is an impressive discriminant. There are 198 tracks, but almost all are within the steeply falling peak at low p_T due to hadronic background, reaction (6). All but one of the other tracks are classified as either tau or charm decays following the multivariate analysis outlined in the next section.

For Short decays, all the cuts were the same but one: the kink angle α cannot be defined since the parent direction is unknown. Here the kink angle was replaced by the "minimum kink angle", obtained by extrapolating the daughter track back to the steel plate and placing the "decay vertex" at the point where this extrapolation intersects the downstream face of the plate. This was the most conservative assumption, since it also minimized the transverse momentum assigned to the decay.

Only events selected by secondary vertex analysis detailed above were submitted to the multivariate analysis employed to determine the probability that individual events represented one of the following interaction types, each with a one-prong or a three-prong secondary vertex:

1. ν_τ CC events, reaction (1).
2. Charm production, reaction (5).
3. Neutrino NC events with a secondary hadron interaction, reaction (6).

No other physical process, subject to the topological and kinematical cuts above, was deemed to be a significant part of the background.

A set of quantities was chosen that could be easily and unambiguously measured in the emulsion data (supplemented by spectrometer information) and that could discriminate between the three hypotheses. Note that all these quantities are independent of the neutrino production and interaction processes. For n parameters, an n-dimensional probability density distribution for each hypothesis was computed using Monte Carlo generated events. Then the relative probability of event k sampled from the distribution of hypothesis i can be written as

$$P(\{x_k\}|i) = \frac{\mathcal{W}_i \mathcal{P}(\{x_k\}|i)}{\sum\limits_j \mathcal{W}_j \mathcal{P}(\{x_k\}|j)} \tag{8}$$

where $\{x_k\}$ is a set of parameters describing event k, $\mathcal{P}(\{x_k\}|i)$ is the probability density function for hypothesis i evaluated for x_k determined from the data, and $\mathcal{W}_i$ is the prior probability of the event being an i-type event. Note that the $\mathcal{W}_i$ are independent of $\{x_k\}$, and give the probability of a neutrino interaction of type i occurring within the emulsion fiducial volume using full MC simulation starting with neutrino production in the beamdump through its interaction in the emulsion target.

The parameter set $\{x_k\}$ for events selected as tau candidates included L_{dec}, α, p_d, θ_p, and $\sum b_d$, introduced above. In addition, $\Delta\phi$ was added, which represents the angle in the plane transverse to the neutrino beam between the parent direction and the vector sum of unit vectors of the remaining tracks at the primary vertex, expected to peak at 180° for ν_τ CC events, and to distribute uniformly for the other two hypotheses.

Hence, for one-prong decay candidates resulting from the Long-decay search, the set $\{x\} = \{L_{dec},\ \alpha,\ p_d,\ \theta_p,\ \Delta\phi\}$ was used, and $\{x\} = \{L_{dec},\ \theta_p,\ \Delta\phi,\ \sum b_d\}$ was used for three-prong decays.

Simulated distributions used as input to the multivariate method are illustrated in Figures 12-14 for all three hypotheses. Fig. 12 shows the $\Delta\phi$ angle in the transverse plane, used for both one- and three-prong topologies, which discriminates very strongly against both charm and hadronic-interaction background. Fig. 13 shows the α decay angle used for the one-prong topology, which discriminates strongly against the hadronic-interaction background, and provides modest discrimination against charm. Fig. 14 shows $\sum b_d$, sum of the daughter-track impact parameters, used for the three-prong topology. This quantity is related to ct for this event, where t is this parent's lifetime in its rest frame. Since τ-lepton has shorter lifetime than charmed mesons, $\sum b_d$ discriminates very strongly against the hadronic-interaction background, and provides strong discrimination against charm. Note that these one-dimensional distributions do not provide information about correlations among the multivariate parameters which are taken into account in the calculation.

The multivariate analysis was also used for events from the Short-decay search. Here, the parent direction is unknown, and hence θ_p, α and $\Delta\phi$ are unkown. The true decay point must have been in the same steel plate that contained the interaction vertex, lying on a line made by projecting the candidate daughter track upstream. Along this line within the steel, the parameters L_{dec}, α, θ_p, and $\Delta\phi$ vary continuously, so that probabilities for the three hypotheses also vary. To make a definite and conservative estimate, the values of all three probabilities were measured at the point along the line where the tau-hypothesis probability was minimum.

Table I summarizes the prior probabilities for both kink and trident topologies and different materials of the emulsion target. Resulting hypothesis probabilities for the ν_τ event candidates are presented in Section IX D below.

C. Decay search efficiencies

The effect of cuts applied during the secondary vertex search was determined by Monte Carlo calculation for all three hypotheses, tau, charm, and hadronic interaction. The secondary-vertex search efficiency was checked by using secondary hadronic interactions found as a byproduct of the track-by-track electron ID scans. The number of interactions expected has a well-understood value depending on path length in a given material (emulsion, steel or plastic). The number of interaction vertices of all multiplicities was estimated to be 31. The total number of found interactions was 27, yielding an efficiency of 0.87, consistent with a Monte Carlo derived efficiency of 0.86.

The fractions of events remaining after selections described in Secions VIII A and VIII B 1 are listed in Table II. The estimate for the overall systematic uncertainties in these efficiencies is 5% of the value.

IX. SURVEY OF DATA

A. Expected composition

The expected number of interactions for reactions (2) - (4) was predicted using the DONuT Monte Carlo simulating the same event-selection procedure that was applied to the data. Charged-current ineractions of all flavors were selected by identifying a lepton at the primary vertex. All neutrino interactions without an identified lepton were considered to be "effective neutral-current" events, $\mathrm{NC}_{\mathit{eff}}$. These $\mathrm{NC}_{\mathit{eff}}$ events therefore included CC events with a lepton that escaped detection. Table III shows the expected number of events of all four interaction types. Note that although the prompt and non-prompt components (see Section II) are separated in the simulation, they are not distinguishable in the data.

B. ν_μ CC events

The identification of muons using the spectrometer was straightforward and efficient, so this category of interactions was considered the most reliable. The number of ν_μ CC events found was 225 events, which gives the fraction of ν_μ CC to the total (578) as 0.39 ± 0.03.

The fraction of prompt ν_μ CC events was estimated both by Monte Carlo and from the data. Averaging over several algorithms, the MC estimate is 0.61 ± 0.03. An estimate from combining results from analyses based on data (number of ν_e CC interactions, fitting to the muon spectrum and data taken with a half-density beamdump) gives 0.59 ± 0.06. The estimated number of prompt ν_μ CC interactions is thus 133 ± 16.

The ratio of the number of $\overline{\nu}_\mu$ interactions with outgoing μ^+ to the number of ν_μ interactions with μ^- was computed from ν_μ and $\overline{\nu}_\mu$ cross sections taking into account detector efficiency and acceptance. The resulting expected ratio was 0.63. The same fraction determined in the 578-event data sample was 0.67 ± 0.08. Using this measured ratio, the ratio of integrated $\overline{\nu}_\mu$ and ν_μ fluxes was found to be 1.05 ± 0.13.

There are three events in the located sample that have two identified muons. One event has muons of opposite sign with one from the primary interaction vertex and the other from a secondary decay vertex. This event is identified as a ν_μ CC interaction producing a charmed meson. The other two dimuon events have same-sign tracks, where one of the tracks is likely a charged π decaying in-flight.

C. ν_e CC events

The expected mean energy of outgoing electrons in ν_e CC interactions was 52 GeV, with 22% of events having electron energies below 20 GeV. Approximately 15% of NC events have at least one electron with energy less than 20 GeV. Therefore, a low-energy cut is applied to the electron sample to reduce background from events that are not ν_e CC events. Table IV summarizes the result of a Monte-Carlo-based study to optimize this cut and to estimate the NC background as a function of energy. For cuts of 18 GeV and higher, there is little change in signal-to-background ratio and a cut of 20 GeV was chosen. A total of 120 ν_e CC and NC$_{eff}$ events passed the cut. The NC$_{eff}$ background fraction is estimated in Table IV to be 0.174, so the best estimate for the number of ν_e CC events (with a 20-GeV electron cut) is given as $120 \times (1 - 0.174) = 99 \pm 9$, as determined by the electronic detector data. To compare this number to the second identification method which follows, it must be divided by the electronic identification efficiency (0.80), yielding 124 ± 11.

The set of events with electrons identified in the emulsion was analyzed independently. There were 82 events with primary electrons found in the emulsion data alone. Of these, 62 electrons passed the 20 GeV minimum energy cut. The electron-identification efficiency of this procedure was found to be independent of energy. The number of ν_e CC, corrected by the efficiency, was $62/0.66 = 94 \pm 12$.

D. ν_τ CC events

The methods of selecting the ν_τ events described in Section VIII were applied to the 578 located events. The multivariate analysis (Section VIII B 2) was performed for each selected event. Events with $P(\tau) > 0.5$ are listed in Table V. We estimate the number of ν_τ, charm, and hadronic interaction events in our final sample by summing up the hypothesis probabilities in Table V, yielding 7.5 ν_τ events, 1.26 charm events, and 0.22 hadronic interactions.

The charm and hadronic-interaction backgrounds can also be estimated in the tau sample using one-dimensional cuts on Monte Carlo events without any reference to the correlations between variables. This simpler analysis gives an estimate of the background from charm decays and hadronic interactions in the nine selected events as 1.1 and 0.9 events, respectively. In comparing the results between the two analyses, it is important to note that the multivariate method accounts for correlations between parameters and results depend on the particular set of candidate events. This last point is significant due to the small number of tau events. The similarity of the charm background from the two analyses demonstrates the similarity in the topological signature of tau and charm decays. The hadronic interaction background, however, shows little correlation between parent track length and 'decay' (interaction) topology, and simple one-dimensional cuts overestimate this background.

E. Charm production in neutrino interactions

Integrating over the expected neutrino energy spectrum, the average charm production fraction, normalized to the number of ν_μ and ν_e CC interactions, is 0.066 ± 0.008 [11]. This fraction includes production of D^0, D$^\pm$, D$_s$, and Λ_c. Including only charged charmed hadrons reduces the fraction to 0.028 ± 0.006. The expected number of charged charm events is the product of the total number of located events (578), the fraction of CC events (0.62), the efficiency for observing the secondary decay (0.45 ± 0.05) and the charged charm fraction (0.028). The result is 4.5 ± 1.0 events, where the error represents the uncertainties in cross sections and branching ratios. The observed number of charged charm events in our sample is 7 events, with an estimated background level of 2.2 events, which is consistent with our prediction.

X. NU-TAU CROSS SECTION

A. Analyses

Two methods were used to measure the cross section for ν_τ-nucleon CC interactions. The primary analysis determined the ratio of the ν_τ-nucleon cross section and the ν_e-nucleon or ν_μ-nucleon cross section. Systematic uncertainties in neutrino production that affected all flavors equally canceled in the relative measurement. Electronic triggering efficiencies and neutrino interaction selection efficiencies were high and for CC events showed no dependence on flavor. However, some corrections applied to the data did not cancel, and their uncertainties contribute to the systematic error. Since only the prompt ν_μ are relevant in the relative cross section calculation, the uncertainty in the prompt fraction was included in the systematic error of the $\sigma(\nu_\tau N)$ to $\sigma(\nu_\mu N)$ ratio. Similarly, the systematic uncertainty related to the energy cut and the NC background subtraction in the ν_e sample was included in the $\sigma(\nu_\tau N)$ to $\sigma(\nu_e N)$ ratio. The ν_τ analysis required the secondary vertex search, and this efficiency (0.46) is applied to the ν_τ events.

The second technique measured the absolute cross section for ν_τN CC interactions. All electronic, event selection and analysis efficiencies appear explicitly in the calculation.

The cross section calculations required an estimate for the number of neutrino interactions in the emulsion target, corrected for efficiency and acceptance. It was important to account for correlations between acceptance and energy. The number of interactions of each flavor in the experiment can be written as

$$N_{\text{int}} = \frac{N_\nu^{\text{tgt}}}{N_{\text{pot}}} \cdot N_{\text{pot}} \cdot \varepsilon \cdot \frac{\sigma^{\text{const}}}{Area} \cdot \frac{M_{\text{tgt}}}{m_{\text{nucleon}}} \cdot \frac{f}{N_\nu^{\text{MC}}} \sum EKTt = \sigma^{\text{const}} \varepsilon C f \left\langle \sum EKTt \right\rangle \tag{9}$$

where the sum is over neutrinos generated by Monte Carlo in the beamdump with energy E, and with kinematic suppression factor $K(E)$. The binary T was equal to one if the neutrino passed within the target fiducial volume and the binary t was equal to one if the interaction generated a trigger. The number of neutrinos generated in the Monte Carlo is denoted by N_ν^{MC} and the number passing through the emulsion is N_ν^{tgt}. The area is taken to be the size of the emulsion, 50 cm $\times$ 50 cm. For the Monte Carlo events, the simulated trigger also incorporated the muon identification for ν_μ interactions. The electron identification, with its efficiencies, was not incorporated directly into t but it, as well as other electronic and analysis efficiencies, were incorporated into ε. The number of protons accumulated in the beamdump (N_{pot}) and the fraction of the neutrino flux (f) intercepting the emulsion are explicitly shown. The quantity C incorporates the energy-independent factors and it depends on neutrino flavor. The angle brackets indicate that the mean value of the sum of the products is used. The Monte Carlo gives f and the mean value of the sum directly and the constants of Eq.(9) are incorporated into C. The values of C and the sum that were used in this analysis are listed in Table VII.

The total CC cross sections per nucleon can be written

$$\sigma_{\nu_\ell} = \sigma_{\nu_\ell}^{\text{const}}\, E\, K\,(E)\,, \qquad \ell = e, \mu, \tau \tag{10}$$

where $\sigma_{\nu_\ell}^{\text{const}}$ is the energy-independent factor of the cross section of flavor ℓ, and K gives the part of the tau-neutrino cross section that depends on kinematic effects due to the τ-lepton mass (see Fig. 15). In the DONuT energy range (Fig. 2), the factor K can be safely taken to be unity for ν_e and ν_μ CC interactions. With this notation, the relative cross sections can be written,

$$\frac{\sigma_\tau^{\text{const}}}{\sigma_\ell^{\text{const}}} = \frac{N_\tau^{\text{exp}}}{N_i^{\text{exp}}} \cdot \frac{C_\ell}{C_\tau} \cdot \frac{f_\ell \left\langle \sum ETt \right\rangle_\ell}{f_\tau \left\langle \sum EKTt \right\rangle_\tau} \cdot \frac{\varepsilon_\ell}{\varepsilon_\tau}, \qquad \ell = e, \mu \tag{11}$$

The ε_i denote efficiencies for lepton identification only. The efficiency of the secondary vertex search is included in ε_τ.

The absolute ν_τ cross section is computed from the following expression,

$$\sigma_\tau^{\text{const}} = \frac{N_\tau^{\text{exp}}}{\varepsilon_{\text{TOT}} \cdot C_\tau \cdot \left(f \left\langle \sum EKTt \right\rangle\right)_\tau} \tag{12}$$

where ε_{TOT} is the product of all experimental efficiencies

$$\varepsilon_{\text{TOT}} = \varepsilon_{\text{FS}} \cdot \varepsilon_{\text{trig}} \cdot \varepsilon_{\text{loc}} \cdot \varepsilon_\tau. \tag{13}$$

The efficiencies in Eq. (13) are as follows: filtering and scanning (0.85 ± 0.06), trigger with live-time (0.79 ± 0.02), location in emulsion (0.64 ± 0.04), and secondary vertex finding (0.46 ± 0.02), yielding $\varepsilon_{\text{TOT}} = 0.20 \pm 0.02$.

B. Systematic uncertainties

The cross section results from this experiment depend on predicting the neutrino fluxes of each flavor. The value of C_ℓ in Eq. (11) and Eq. (12) depends linearly on the total charm production cross section in pN interactions in the beamdump. And the value of f_ℓ times the term in the brackets depends on the angular distribution of charm in the pN center-of-momentum frame. Most of the systematic uncertainty in the cross section results was due to these two terms. We examine each in more detail.

The factor C_ℓ contains the number of neutrinos produced in the beamdump, so it is sensitive to variations in total cross section, branching ratios and target atomic number effects, which we parameterize by A^α. The relative errors for charm production of ν_e and ν_μ is taken to be the same for both: 0.10 from charm total cross section, 0.16 from branching ratios and 0.14 from the A dependence. We adopt the convention to add the errors in quadrature where values are derived from several sources and not likely to be correlated. This gives a total relative error of 0.23 for C_e and C_μ. The estimated uncertainty in C_τ depends almost entirely on $\mathrm{D_s}$ production and decay. The relative uncertainties are computed to be 0.15, 0.23 and 0.14 for cross section, branching ratio and A dependence, respectively. Added in quadrature, this gives 0.31 for the relative uncertainty in C_τ. In the results for the relative cross section measurement, below, the uncertainty in the A dependence is not included in the second, systematic error.

The factor $f\Sigma EKTt$ is sensitive to kinematic uncertainties in charm production, with the effects manifested in the variation of the parameter n of Eq. (7). Both the neutrino energy (and hence number of interactions) and the fraction of the neutrino flux within the emulsion are affected. We compute the amount of variation in the number of accepted Monte Carlo events and assign it to the systematic error in $f\Sigma EKTt$. We assume $n = 8.0 \pm 0.8$ for both D_s^+ and D_s^- production, but in computing the relative error, allow n to be different by ± 2.0 for D_s^-. This gives a relative uncertainty of +0.31 and -0.23 in ν_τ production. The uncertainties in $f\Sigma EKTt$ for ν_e and ν_μ were computed analogously, yielding +0.30 and -0.20. The positive uncertainty corresponds to a decrease in n by two units.

For ν_e and ν_μ CC interactions we can estimate $C_{e,\mu}$ from the number of interactions in the data, given the values of $f\Sigma EKTt$ and the efficiencies computed from the Monte Carlo. This provides a systematic check on C. The values are $C_e = 1.47 \times 10^{40}\mathrm{cm}^{-2}$ and $C_\mu = 1.79 \times 10^{40}\mathrm{cm}^{-2}$ (prompt muons only). These are compared with 1.64×10^{40} and 1.55×10^{40}, respectively from Table VII, which were extracted from Monte Carlo simulations with values of the parameter n discussed above. This indicates that the systematic uncertainty in the charm cross sections is within the values (+0.30, -0.20) estimated above.

C. Results

The relative cross sections were obtained from Eq. (11) using the observed number of interactions, corrected by efficiency and kinematic factors. Inserting the values from Table VIII yields

$$\frac{\sigma^{\mathrm{const}}_{\nu_\tau}}{\sigma^{\mathrm{const}}_{\nu_e}} = 1.58 \pm 0.58 \pm 0.91 \quad \text{and} \quad \frac{\sigma^{\mathrm{const}}_{\nu_\tau}}{\sigma^{\mathrm{const}}_{\nu_\mu}} = 1.16 \pm 0.42 \pm 0.65 \tag{14}$$

The first error in the results is the statistical error, the second is the estimated sytematic uncertainty. The systematics of these two results are correlated, since the same assumptions regarding charm production were made for both ν_e and ν_μ production. Therefore, the two cross section may be averaged without introducing other uncertainties. The result is

$$\frac{\sigma^{\mathrm{const}}_{\nu_\tau}}{\sigma^{\mathrm{const}}_{\nu_{e,\mu}}} = 1.37 \pm 0.35 \pm 0.77 \tag{15}$$

The absolute ν_τ-nucleon cross section was computed using the factors of Table VII inserted into Eq. (12):

$$\sigma^{\mathrm{const}}_{\nu_\tau} = 0.72 \pm 0.24 \pm 0.36 \times 10^{-38} \quad \mathrm{cm}^2\,\mathrm{GeV}^{-1} \tag{16}$$

The first error is statistical, the second one systematic.

Lack of knowledge of the charge of the τ lepton implies that the result, Eq. (16), represents an average of ν_τ and $\bar{\nu}_\tau$ cross sections. The measured value of $\sigma^{\mathrm{const}}_{\nu_\tau}$ is to be compared with the average of ν_μ and $\bar{\nu}_\mu$ cross section factors, 0.51×10^{-38} cm^2 [12], assuming equal fluxes of neutrinos and antineutrinos in the DONuT beam. Hence, the ν_τ result, Eq. (16), is consistent with Standard Model assuming lepton universality. As discussed in Section IX B, the flux of neutrinos in the DONuT beam is approximately equal to the flux of antineutrinos, which has been assumed for the results given above. The actual value of the ratio of $\bar{\nu}_\mu$ and ν_μ fluxes in the DONuT beam was measured to be 1.05 ± 0.13. This ν-$\bar{\nu}$ imbalance taken at face value would result in a negligible correction to the relative cross section if one assumes that it applies to all flavors equally. The absolute cross section would be reduced by about 2.5%.

XI. CONCLUSIONS

The identification of a set of likely ν_τ interactions with small background has enabled a first direct measurement of the ν_τ charged-current cross section. The values obtained are consistent with the Standard Model expectation of unity for the relative cross sections. Since the uncertainty from hadronic charm production and decay is larger than the statistical error, these results can be improved with better data from charm production experiments.

XII. ACKNOWLEDGMENTS

We would like to thank the support staffs at Fermilab and the collaborating institutions. We acknowldge the support of the U.S. Department of Energy, the Japan Society for the Promotion of Science, the Japan-US Cooperative Research Program for High Energy Physics, the Ministry of Education, Science and Culture of Japan, the General Secretariat of Research and Technology of Greece, the Korean Research Foundation, and the DOE/OJI Program.

[1] M. Perl *et al.*, Phys. Rev. Lett. **35**, 1489 (1975).
[2] C.L. Cowan, F. Reines, F.B. Harrison, H.W. Kruse, A.D. McGuire, Science **124**, 103 (1956).
[3] G. Danby *et al.*, Phys. Rev. Lett. **9**, 36 (1962).
[4] DONuT Collaboration, K. Kodama *et al.*, Phys. Lett. B **504**, 218 (2001).
[5] B. Lundberg, K. Niwa, and V. Paolone, Ann. Rev. Nucl. Part. Sci. **53**, 199 (2003).
[6] DONuT Collaboration, K. Kodama *et al.*, Nucl. Instr. Meth. A **493**, 45 (2002).
[7] DONuT Collaboration, K. Kodama *et al.*, Nucl. Instr. Meth. A **516**, 21 (2004).
[8] G. Oleynik *et al.*, *in:* Proceedings of the Conference on Real Time Computer Applications in Nuclear, Particle, and Plasma Physics, Vancouver 1993, p. 348.
[9] S. Aoki, Nucl. Instr. Meth. A **473**, 192 (2001).
[10] DONuT Collaboration, K. Kodama *et al.*, Nucl. Instr. Meth. A **574**, 192 (2007).
[11] J. Sielaff, Ph.D. Thesis, University of Minnesota, Minneapolis, MN, 2001; S.A. Rabinowitz *et al.* (CCFR), Phys. Rev. Lett. **70**, 134 (1993).
[12] W.M. Yao *et al.* (Particle Data Group), J. Phys. G **33**, 1 (2006),
[13] E653 Collaboration, K. Kodama *et al.*, Phys. Lett. B **263**, 573 (1991).
[14] E653 Collaboration, K. Kodama *et al.*, Phys. Lett. B **284**, 461 (1992).
[15] ACCMOR Collaboration, S. Barlag *et al.*, Z.Phys.C **49**, 555 (1991).
[16] LEBC-MPS Collaboration, R. Ammar *et al.*, Phys. Rev. Lett. **61**, 2185 (1988).
[17] E769 Collaboration, G.A. Alves *et al.*, Phys. Rev. Lett. **77**, 2388 (1996).
[18] WA92 Collaboration, M. Adamovich *et al.*, Nucl.Phys. B **495**, 3 (1997).
[19] E789 Collaboration, D.M. Kaplan *et al.*, Int. J. Mod. Phys. A **12**, 3827 (1997).
[20] E789 Collaboration, M.J. Leitch *et al.*, Phys. Rev. Lett. **72**, 2542 (1994).
[21] T. Åkesson *et al.*, Z. Phys. C **72**, 429 (1996).
[22] HERA-B Collaboration, A. Zoccoli *et al.*, Eur. Phys. J. C **43**, 179 (2005).
[23] C. Lourenço and H.K. Wöhri, Phys. Rep. **433** 127 (2006).

TABLE I: Summary of the prior probabilities for the multivariate analysis.

Material	Number of decay prongs	Prior probabilities $\mathcal{W}$ Tau decay	Charm decay	Hadron int.
Emulsion	1	2.7×10^{-3}	1.9×10^{-3}	4.1×10^{-5}
Emulsion	3	2.7×10^{-3}	1.9×10^{-3}	2.0×10^{-4}
Plastic	1	1.6×10^{-2}	1.2×10^{-3}	7.5×10^{-6}
Plastic	3	2.7×10^{-3}	1.9×10^{-3}	6.7×10^{-5}
Steel	1	1.6×10^{-2}	1.2×10^{-3}	5.1×10^{-4}
Steel	3	1.6×10^{-2}	1.2×10^{-3}	5.6×10^{-3}

TABLE II: Efficiencies for identifying the secondary vertex in ν_τ interactions, in charm-producing ν_e and ν_μ interactions, and in ν NC events with secondary hadronic interactions. (Kink-daughter type is given in parentheses.)

Decay Topology	$\nu_\tau \to \tau^-$	$\bar{\nu}_\tau \to \tau^+$	$\nu \to charm$	$\bar{\nu} \to charm$	Hadron interactions
1-prong (Hadron)	0.39	0.39	0.26	0.32	0.72
1-prong (Electron)	0.49	0.51	0.35	0.36	
1-prong (Muon)	0.50	0.54	0.34	0.33	
3-prong decay	0.58	0.62	0.45	0.56	0.84
All	0.46	0.47	0.34	0.40	0.76

TABLE III: Expected composition of the beamdump neutrino beam. The distinction of ν_μ from prompt (charm decay) and non-prompt (π and K decay) sources can be made only for Monte Carlo. The $\mathrm{NC}_{\mathit{eff}}$ category includes all events not classified as charged-current.

	ν_e CC	ν_μ CC prompt	ν_μ CC non-prompt	ν_τ CC	$\mathrm{NC}_{\mathit{eff}}$
MC fraction	0.181	0.199	0.159	0.018	0.442
MC fraction $\times$ 578	105	115	92	10	256
Data	120	225		9	224
Difference	15 ± 15	18 ± 21		-1 ± 4	-32 ± 22

TABLE IV: Results of a systematic study of classifying ν_e CC events as a function of electron energy. N_e^{data} includes both ν_e CC events and a background of $\mathrm{NC}_{\mathit{eff}}$ events misidentified as ν_e CC events. The last column gives the estimated true number of CC ν_e events after subtracting background and correcting for efficiency, and should be constant in energy if systematics are small. Events with energy less than 20 GeV were rejected from the CC ν_e set and therefore assigned to the $\mathrm{NC}_{\mathit{eff}}$ set.

Energy cut (GeV)	N_e^{data}	$N^{\mathrm{data}}(\mathrm{NC}_{\mathit{eff}})$	$\varepsilon(\nu_e\mathrm{CC})$	$\mathrm{NC}_{\mathit{eff}}$ bkg	N_e^{corr}
15	144	207	0.747	0.239	154
18	134	217	0.693	0.194	161
20	120	231	0.635	0.174	166
25	104	247	0.573	0.160	163
30	91	260	0.514	0.153	165

TABLE V: List of ν_τ events with parameters used in the analyses and the result of the multivariate analysis. (†)Event 3139/22722 was a Short decay so the probability values listed are at the tau probability minimum.

Event	Daughter	L_{dec} (mm)	α (rad)	b_d (μm)	$\Delta\phi$ (rad)	θ_p (rad)	p_d (GeV/c)	$P(\tau)$	$P(c)$	$P(int)$
3024/30175	e	4.47	0.093	416	1.09	0.030	5.2	0.53	0.47	0.00
3039/01910		0.28	0.089	24	2.71	0.065	4.6	0.96	0.04	0.00
3140/22143	μ	4.83	0.012	60	1.67	0.040	22.2	0.97	0.03	0.00
3333/17665	e	0.66	0.011	8	2.84	0.016	59	0.98	0.02	0.00
3024/18706	e	1.71	0.014	23	2.96	0.043	50	1.00	0.00	0.00
3139/22722†		0.44	0.027	12	1.71	0.155	15.8	0.50	0.29	0.21
3296/18816		0.80	0.054	38	1.74	0.140	5.0	0.71	0.29	0.00
			0.190	148			1.3			
			0.130	112			1.9			
3334/19920		8.88	0.017	147	3.11	0.041	11.6	1.00	0.00	0.00
			0.011	98			15.7			
			0.011	94			3.2			
3250/01713		0.83	0.133	110	2.83	0.028	1.3	0.87	0.12	0.01
			0.192	161			2.4			
			0.442	355			0.5			
Total								7.5	1.26	0.22

TABLE VI: Quantities used in the analysis to compute neutrino cross sections. The charm production cross section in a material of atomic number A is assumed to be proportional to A^α. The differential cross section is assumed to be given by Eq.(7).

Quantity	Value
$\sigma(\mathrm{pN} \to \mathrm{D}^\pm \mathrm{X})$	21 ± 2 μb
$\sigma(\mathrm{pN} \to \mathrm{D}^0 \mathrm{X})$	39 ± 3 μb
$\sigma(\mathrm{pN} \to \mathrm{D}_s \mathrm{X})$	7.9 ± 1.2 μb
$\sigma(\mathrm{pN} \to \Lambda_c \mathrm{X})$	8 ± 5 μb
$\sigma_{tot}(\mathrm{pW})$	1650 mb
α	0.99 ± 0.03
n	8.0 ± 0.8
b	0.83 ± 0.22 (GeV/c)$^{-2}$

TABLE VII: Monte Carlo derived factors in the cross section analysis.

Type	C_ℓ $\times 10^{40}$ cm^{-2}	$f\left\langle \sum EKTt \right\rangle_\ell$ GeV
ν_e	1.64 ± 0.38	$4.62^{+1.41}_{-0.94}$
ν_μ	1.55 ± 0.36	$4.33^{+1.32}_{-0.88}$
ν_τ	0.222 ± 0.085	$2.23^{+0.69}_{-0.52}$

TABLE VIII: The values for the factors of Eq. (11) giving the relative cross sections. The number of observed ν_τ interactions is the sum of the probabilities listed in Table V, column 7. The values of C and $f\left\langle \sum EKTt \right\rangle$, columns four and five, are listed in Table VII.

x	$N^{\exp}_{\nu_x}$	$\varepsilon(\nu_x)/\varepsilon(\nu_\tau)$	C_x/C_τ	$f\left\langle \sum \right\rangle_x / f\left\langle \sum \right\rangle_\tau$
τ	7.5			
e	99	1.36 ± 0.08	7.40 ± 3.25	2.07 ± 0.78
μ	138	1.57 ± 0.10	7.01 ± 2.98	1.94 ± 0.71

APPENDIX A: CHARM AND TAU PRODUCTION IN 800-GEV PROTON-NUCLEON INTERACTIONS

The majority of the neutrino flux at the DONuT emulsion target originated in charm decays from interactions of 800 GeV protons in the tungsten alloy beamdump. This flux was estimated from results of hadronic charm production in fixed-target experiments. The results from three experiments were used in the following way. First, we fix the absolute rate of charm production in 800 GeV proton-nucleon using inclusively produced D^0 cross sections from Ref. [13][16][22][23]. The value of the D^0 cross section from [22] was scaled from 920 GeV to 800 GeV, a factor of 0.84, using Pythia with CTEQ6L structure functions before averaging [23].

We then make the assumption that the ratio of any charm particle cross section to D^0 from the same experiment is independent of energy and beam particle. The product of the weighted average of these ratios and the 800 GeV D^0 cross section gives our estimate for the inclusive production cross sections for $D^{\pm}$, D_s. Table IX lists the experimental results used in this analysis. Table X gives the values for the ratios of charm species to D^0 used. Note that the ratio of the ν_μ to ν_e CC cross section ratio does not depend on the numbers used in Table X. Input values used in the cross section analysis, including charm cross sections are listed in Table VI.

The simulated charm produced in the beamdump are forced to decay semi-leptonically (or leptonically) with the branching fractions listed in Table XII. The charm was produced in the Monte Carlo using the simple form of Eq. (7), with values of n given in Table XI. The value of b was set to 0.9 ± 0.1.

The simulation of charm production, described above, is appropriate for 800 GeV pN interactions. Charm particles were also produced in hadronic cascade showers in the beamdump, which we call secondary charm production. This secondary production was modeled by the Monte Carlo in a manner similar to non-prompt neutrino generation. Instead of simulating decays of πs and Ks after each GEANT step, a charmed meson was generated and weighted according to production cross sections via an energy-dependent function similar to the $K(E)$ function shown in Fig. 15. The number of neutrino interactions from secondary charm decays relative to total was estimated to be 0.075 ± 0.033. This value was applied as a correction to the absolute cross section and was assumed to be independent of flavor.

TABLE IX: The charm cross section results used in the cross section ratios given in Table X, below. The D^0 cross section was obtained from the first three results, pN reactions at high energy. The ratio of $D^{\pm}$ to D^0 was obtained from the results above the line (all pN reactions). The ratio of D_s to D^0 was obtained the results below the line. The resulting cross sections are listed in Table VI.

Ref.	Beam type/ Energy (GeV)	$\sigma(D^{\pm})$ μb/nucl	$\sigma(D^0)$ μb/nucl	$\sigma(D_s)$ μb/nucl
[13]	p/800	$37 \pm 9 \pm 12$	$43 \pm 3 \pm 14$	NA
[16]	p/800	$26 \pm 4 \pm 7$	$22 \pm 8 \pm 6$	NA
[22]	p/920	$29.9 \pm 4.5 \pm 5.7$	$56.3 \pm 8.5 \pm 9.5$	NA
[17]	p/250	$3.3 \pm 0.4 \pm 0.4$	$6.0 \pm 1.4 \pm 0.5$	1.5 ± 1.5
[15]	π/230	$3.2 \pm 0.2 \pm 0.7$	$6.6 \pm 0.3 \pm 1.0$	2.7 ± 0.2
[17]	π/250	$3.6 \pm 0.2 \pm 0.3$	$8.7 \pm 0.7 \pm 0.6$	2.0 ± 0.5
[17]	K/250	3.0 ± 0.4	7.2 ± 1.1	3.0 ± 0.9
[17]	p/250	3.2 ± 0.5	5.4 ± 1.4	1.5 ± 1.5
[18]	π/350	$3.2 \pm 0.1 \pm 0.3$	$7.8 \pm 0.14 \pm 0.5$	1.3 ± 0.4

TABLE X: The weighted average ratio of $D^{\pm}$ and D_s cross sections to D^0 for results listed in Table IX.

Avg. $\frac{\sigma(D^{\pm})}{\sigma(D^0)}$	Avg. $\frac{\sigma(D_s)}{\sigma(D^0)}$
0.51 ± 0.06	0.203 ± 0.031

TABLE XI: The production parameter n of Eq. (7) used to generate charm particles in the Monte Carlo. The error on the values gives the range of n used in the estimating the systematic uncertainty.

Charm particle	n
D^0	6.0 ± 0.6
$\overline{\mathrm{D}}^0$	7.0 ± 0.6
D^+ and D^-	5.0 ± 0.6
D_s^+ and D_s^-	8.0 ± 0.8
Λ_c^+	2.5 ± 0.5
Λ_c^-	8.0 ± 2.0

TABLE XII: Leptonic braching fractions of charm and tau used in the analysis

$BR(D_s \rightarrow \nu_e\ X)$	0.08 ± 0.055
$BR(D_s \rightarrow \nu_\tau\ X)$	0.064 ± 0.015
$BR(D_s \rightarrow \nu_\mu\ X)$	0.08 ± 0.055
$BR(D^\pm \rightarrow \nu_e\ X)$	0.172 ± 0.019
$BR(D^\pm \rightarrow \nu_\tau\ X)$	7×10^{-4}
$BR(D^\pm \rightarrow \nu_\mu\ X)$	0.16 ± 0.03
$BR(D^0 \rightarrow \nu_e\ X)$	0.069 ± 0.003
$BR(D^0 \rightarrow \nu_\mu\ X)$	0.066 ± 0.008
$BR(\Lambda_c \rightarrow \nu_e\ X)$	0.021 ± 0.007
$BR(\Lambda_c \rightarrow \nu_\mu\ X)$	0.020 ± 0.006
$BR(\tau \rightarrow \nu_e\ X)$	0.1784 ± 0.0006
$BR(\tau \rightarrow \nu_\mu\ X)$	0.1736 ± 0.0006

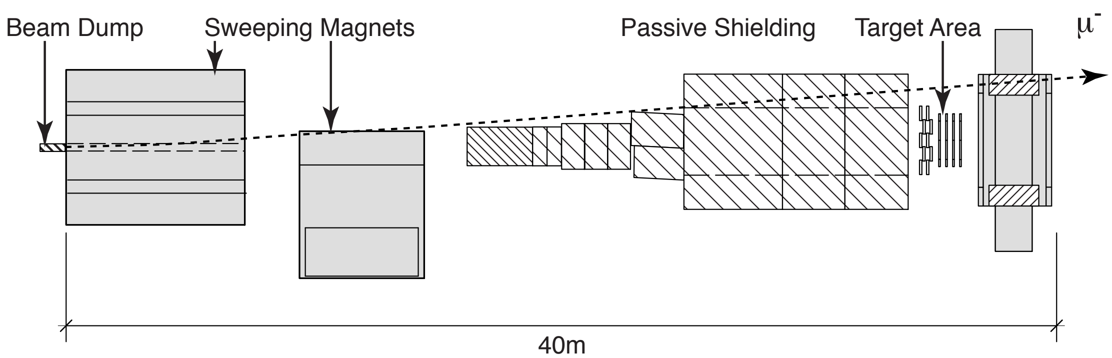

FIG. 1: Schematic plan view of the neutrino beam. The 800 GeV protons are incident on the beamdump from the left. The emulsion modules are located within the target area, 36 m from the beamdump. The trajectory of a 400 GeV/c negative muon is shown. Note that the passive steel shield does not fill the volume occupied by high-energy muons along the plane of the beamline.

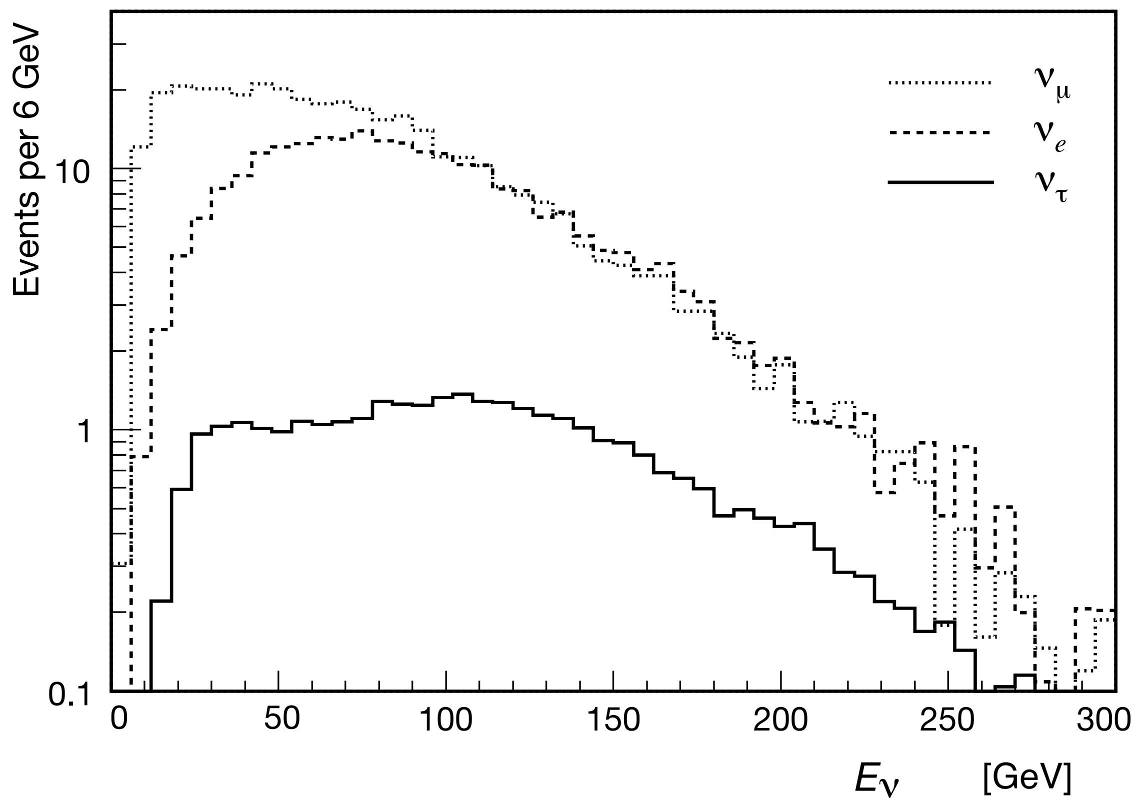

FIG. 2: Calculated energy spectra of neutrinos interacting in the DONuT emulsion target.

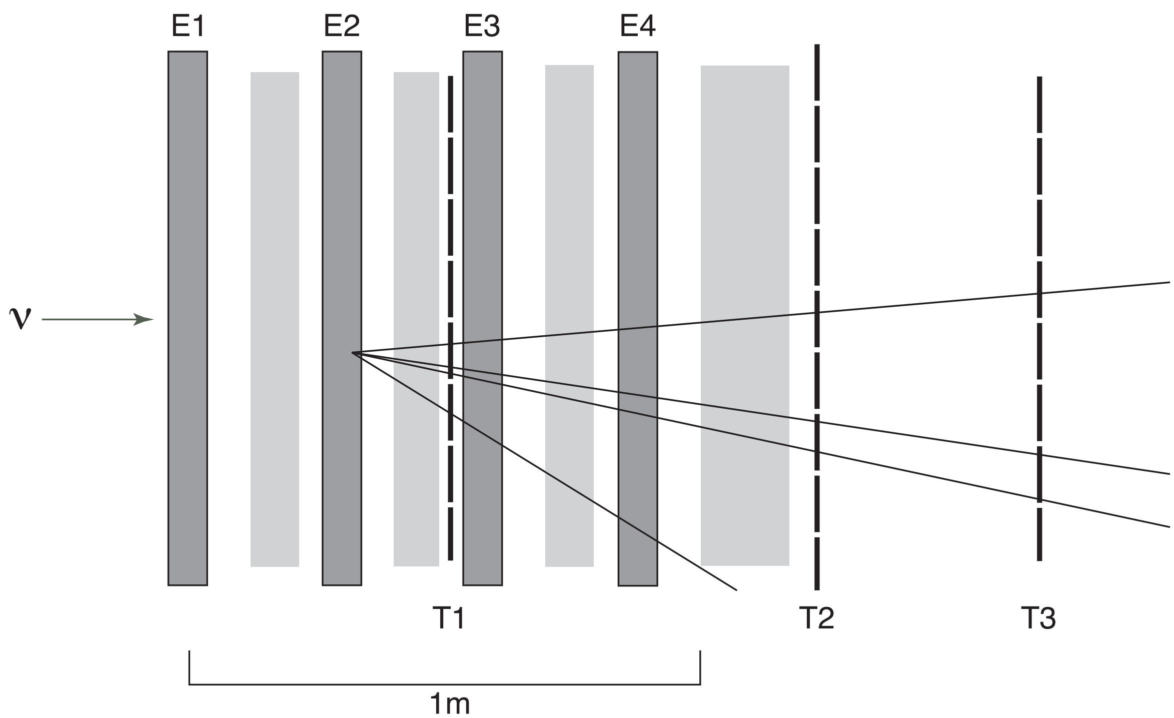

FIG. 3: Schematic plan view of the target region. The emulsion modules are indicated with E labels, the trigger hodoscopes with T labels. The lighter gray areas are occupied by scintillating fiber planes, 44 in total. The paths of charged particles in a typical interaction are superimposed.

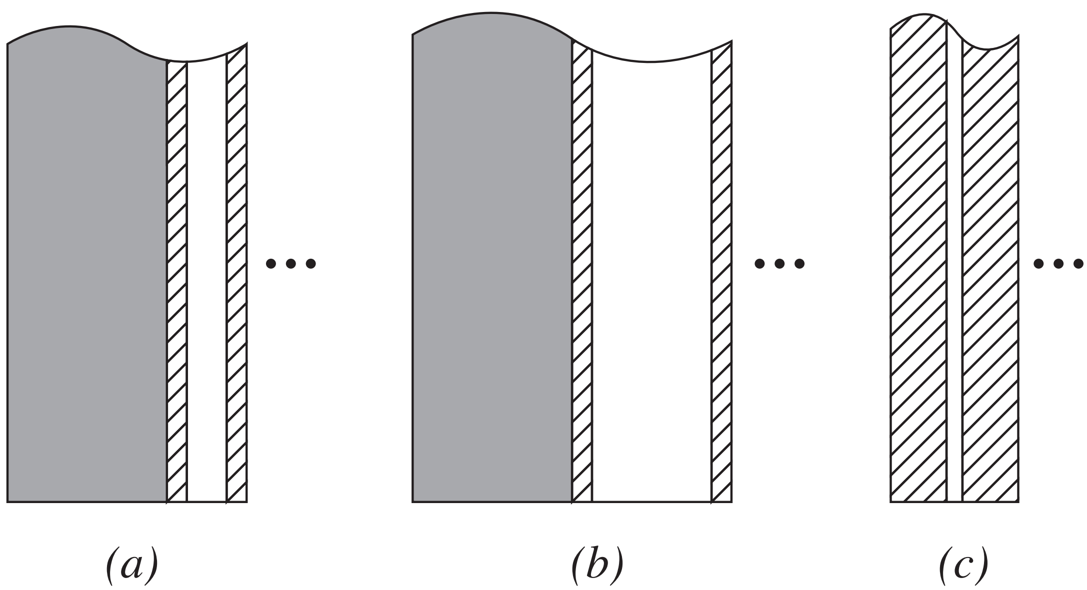

FIG. 4: Emulsion target designs. The ECC designs (a) and (b) used 1-mm thick stainless steel sheets interleaved with emulsion plates using 100 μm thick emulsion layers on a 200-μm plastic base in (a), and 800-μm plastic base in (b). Most neutrino interactions were in the steel. The bulk emulsion type (c) used 350-μm emulsion layers on 90-μm plastic base, without steel. Steel is indicated by shading, emulsion by cross-hatching, the plastic base is unshaded.

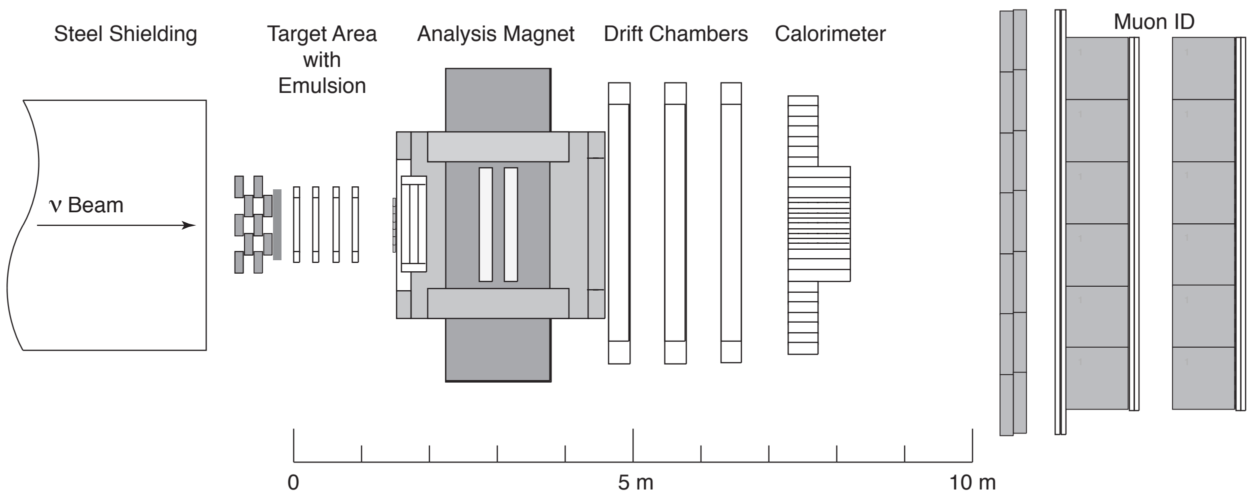

FIG. 5: Schematic plan view of the spectrometer. The neutrinos are incident from the left, emerging from the passive shield. The design is relatively compact, to optimize identification of leptons (muons and electrons).

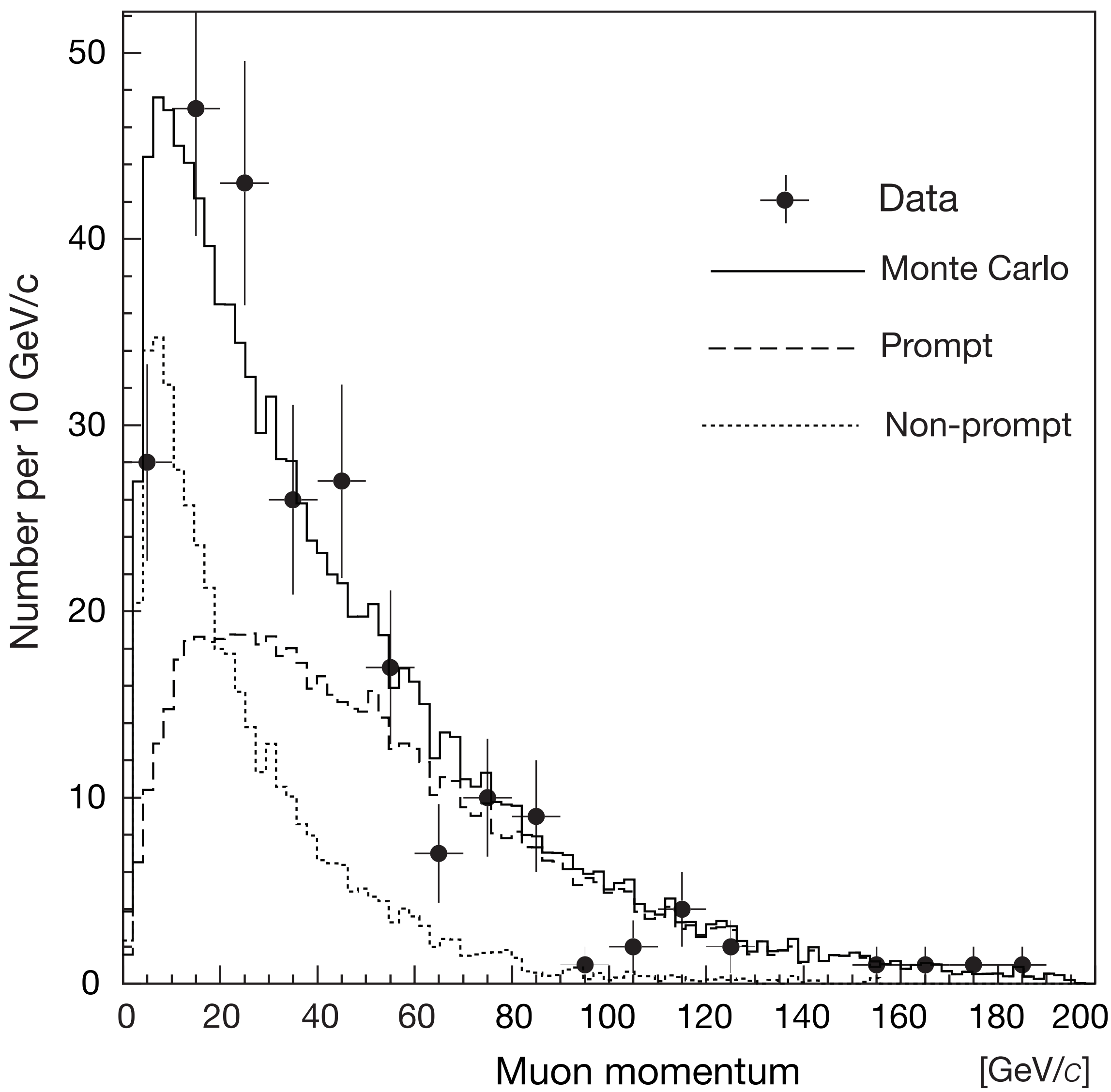

FIG. 6: Muon momentum distribution for the set of 578 located events. The data are shown by solid circles, and Monte Carlo expectation is the solid histogram. Also shown are the expected muon distributions from the two components of the ν_μ flux, prompt (dashed) and non-prompt (dotted) histograms.

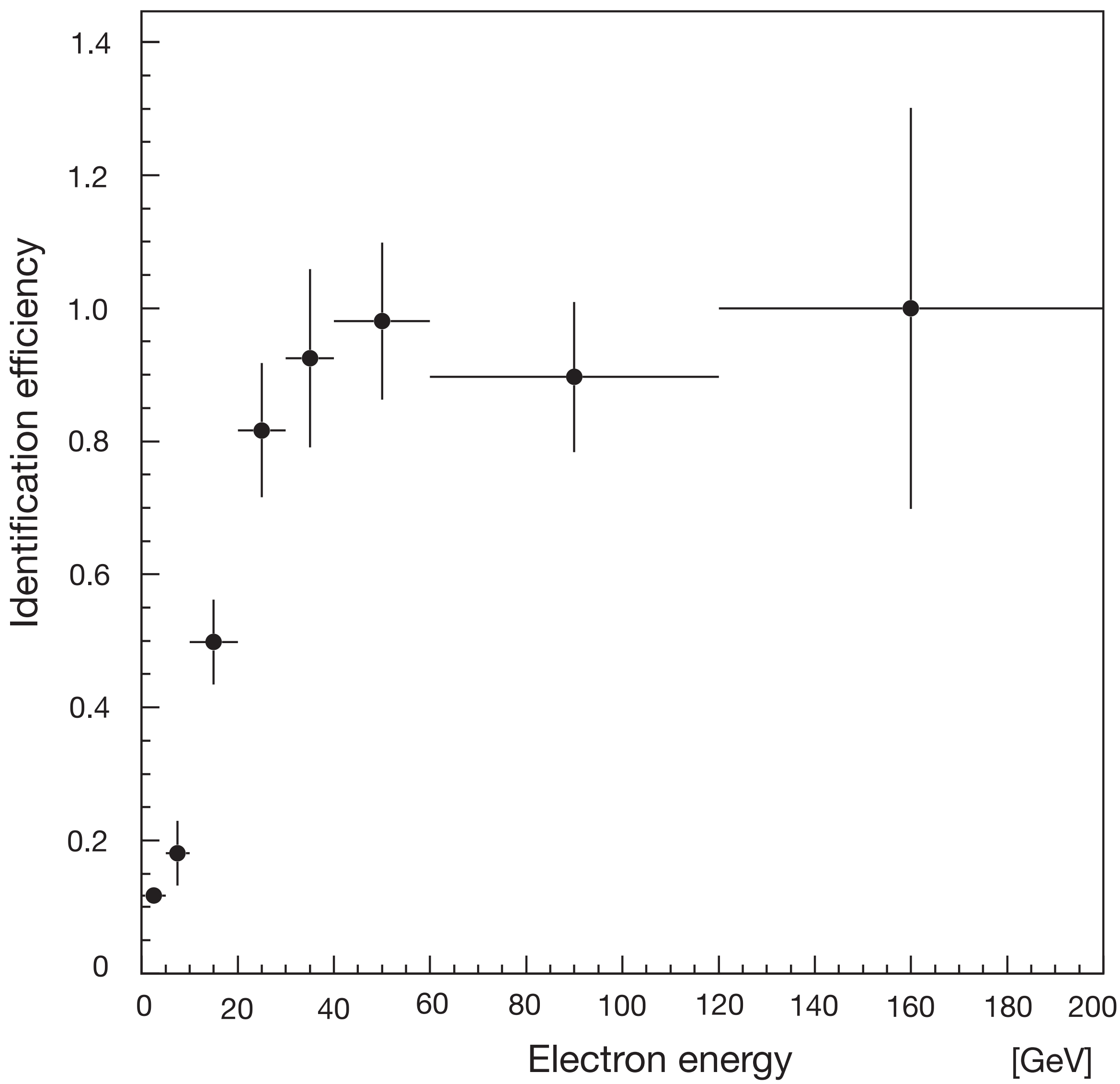

FIG. 7: The electron identification efficiency as a function of electron energy. This analysis used the scintillating fiber detector and the calorimeter.

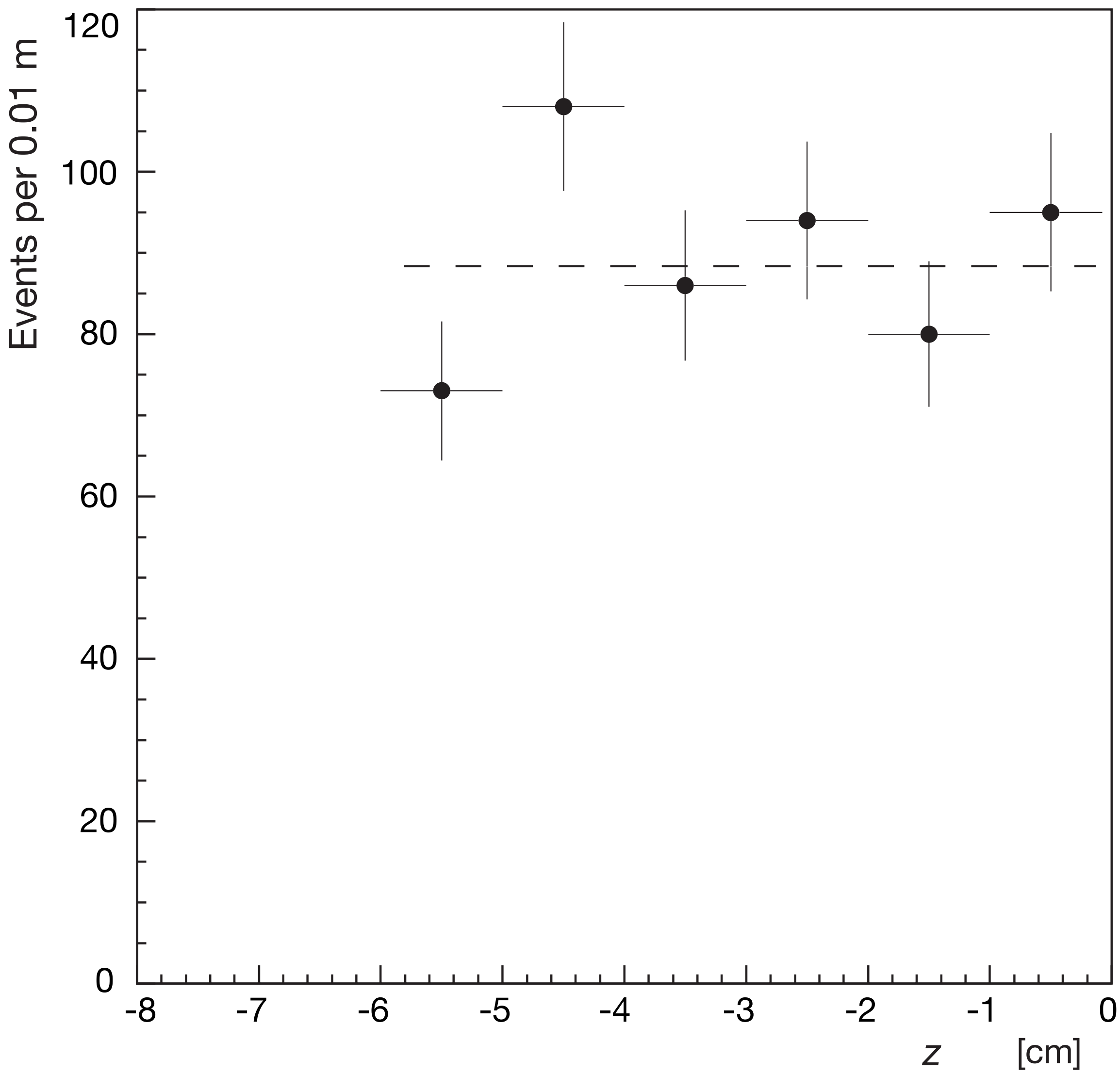

FIG. 8: Number of located events as a function of z, the vertex position measured from the downstream edge of a module along the beam direction. Data from all seven modules are included. Also shown (*dashed line*) is the fit assuming the results are independent of z, yielding a value of 88 with χ^2/dof equal to 1.7.

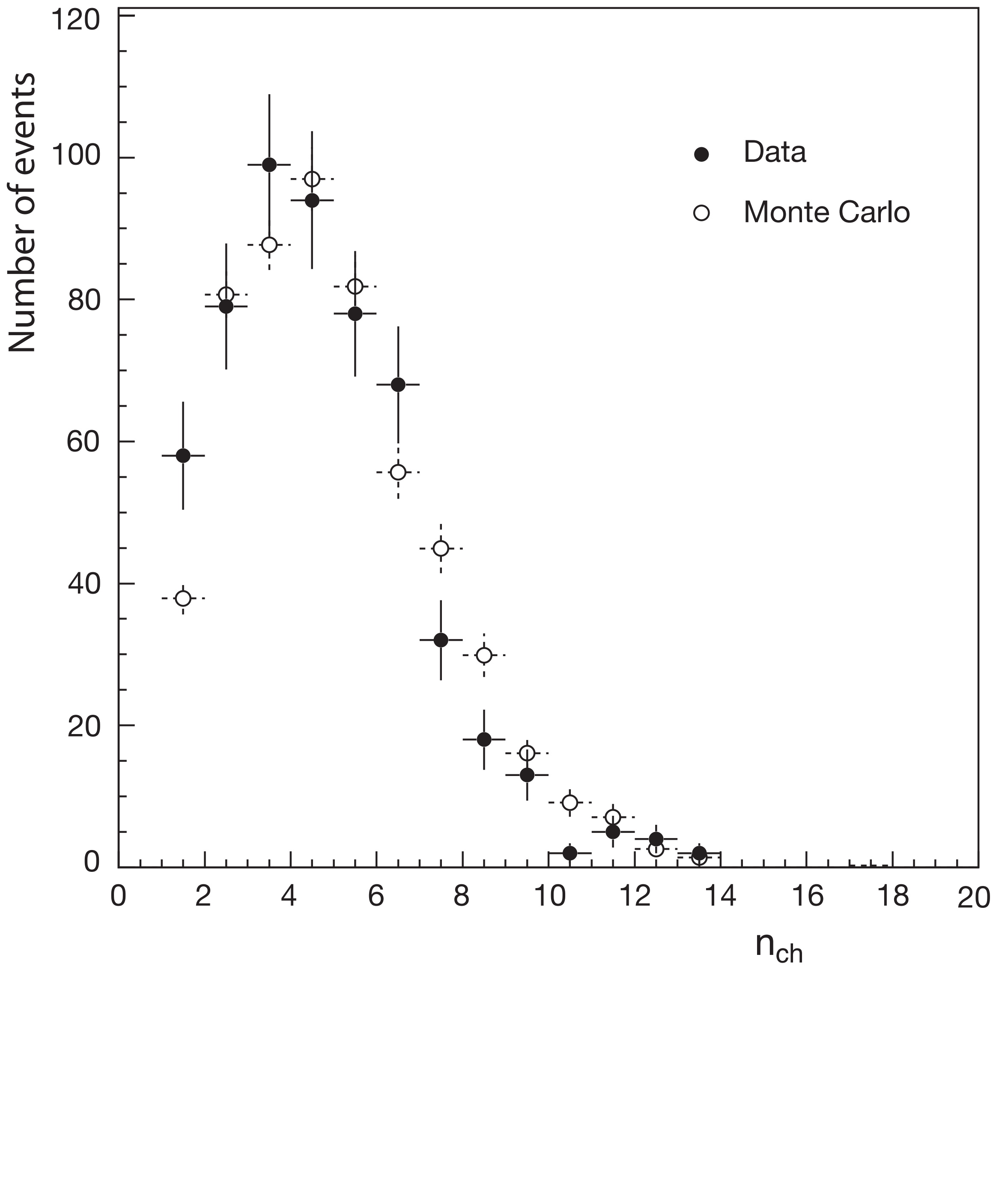

FIG. 9: Charged-particle multiplicity, n_{ch}, at the primary vertex of all the located events. Data is shown by solid circles, Monte Carlo by open circles.

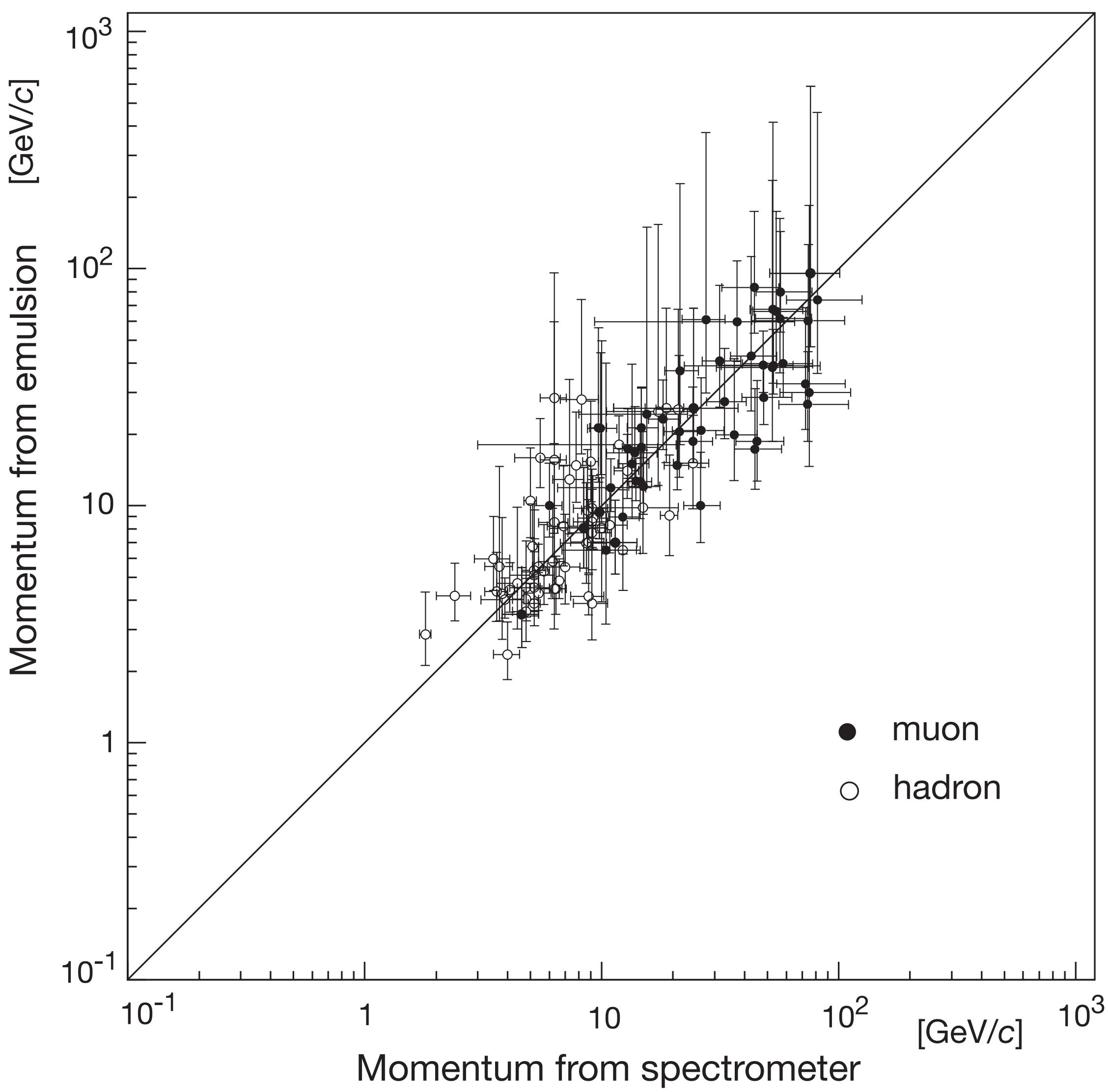

FIG. 10: A comparison between track momenta measured by multiple coulomb scattering in emulsion and by the spectrometer. Although the tracks tagged as muons avoid secondary interactions, the momenta are often at upper limit of measurement in the emulsion.

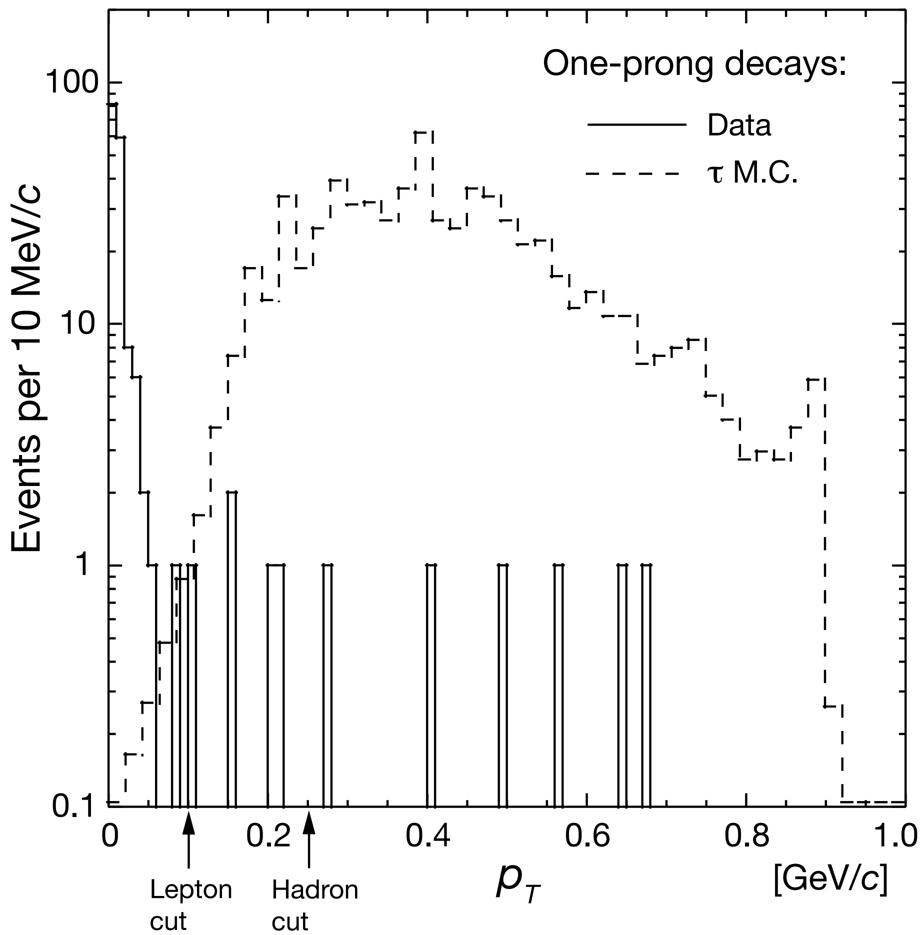

FIG. 11: The distributions of one-prong secondary-vertex events (solid line) after all the topological and kinematic cuts *except* on transverse momentum. Superposed is the expected distribution from τ one-prong decays (dashed line, arbitrary normalization). For τ candidates, the kink transverse momentum must exceed 0.25 GeV/c for $\tau \rightarrow hadron$ or exceed 0.1 GeV/c for $\tau \rightarrow e$ or μ.

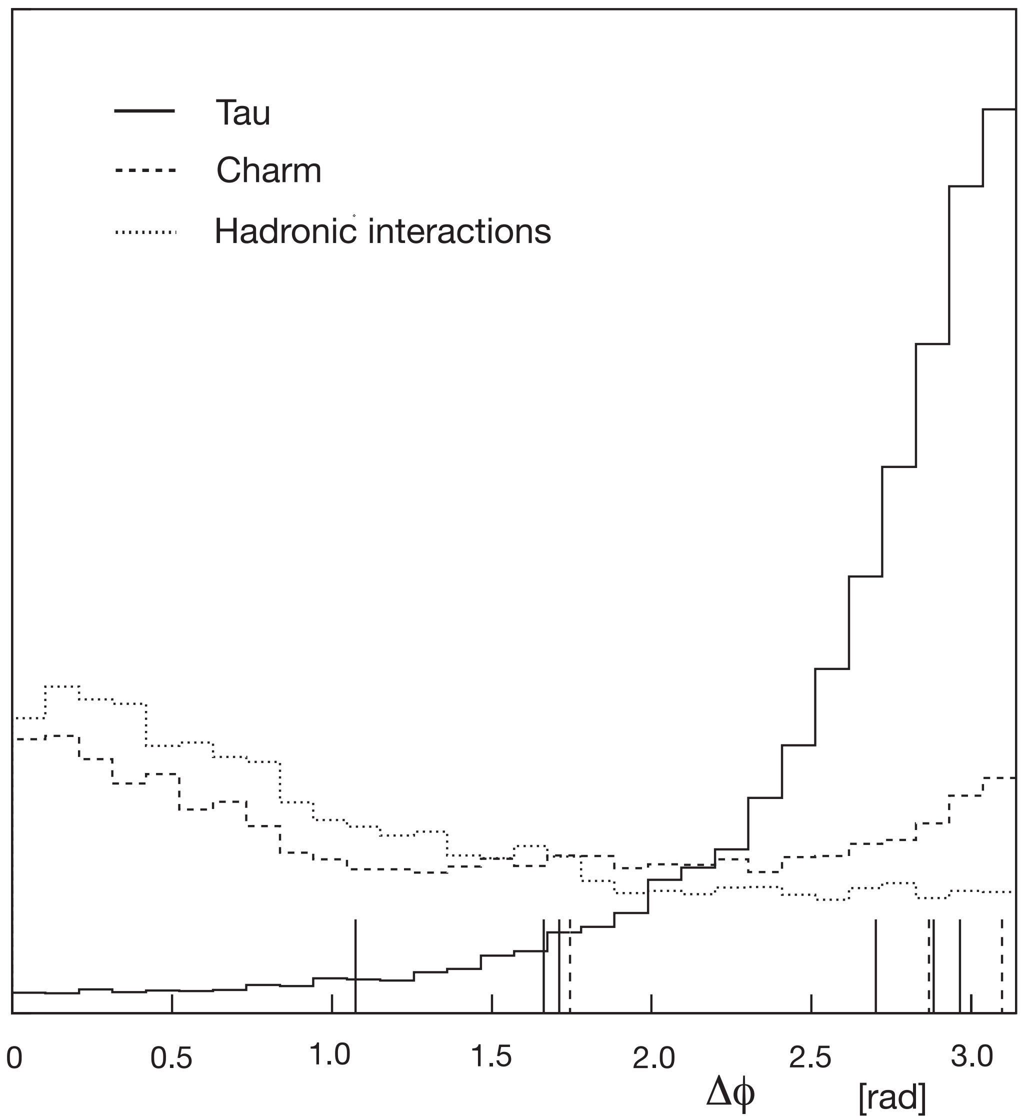

FIG. 12: An example of simulated distributions used as input to the event probability calculation within the multivariate method as applied to all decays. Shown are distributions of the transverse-plane angle $\Delta\phi$ for all three hypotheses under consideration: tau (*solid line*), charm (*dashed line*), and hadronic interactions (*dotted line*). Short vertical lines indicate the values for ν_τ candidate events from Table V for one-prong decays (*solid line*) and three-prong decays (*dashed line*)

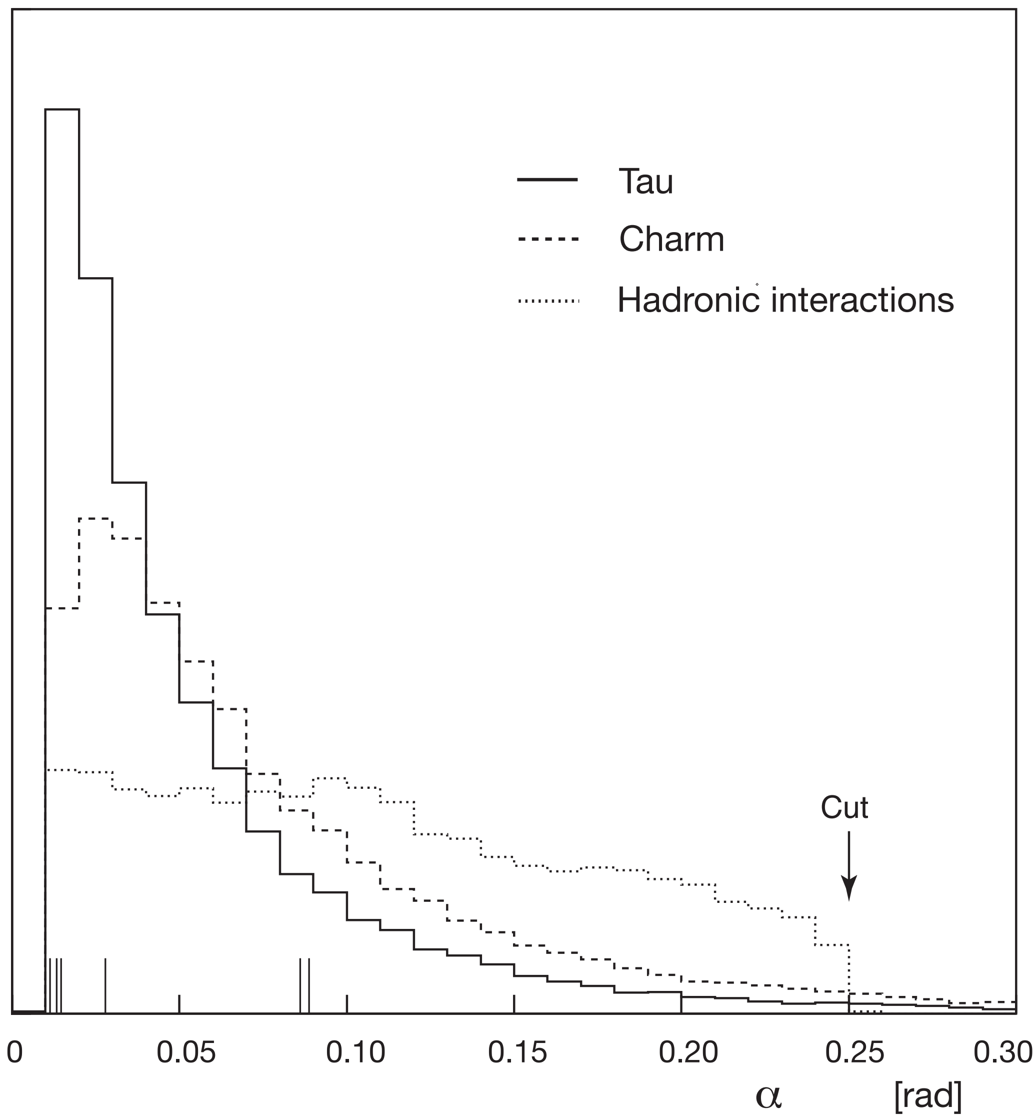

FIG. 13: An example of simulated distributions used as input to the event probability calculation within the multivariate method as applied to one-prong decays. Shown are distributions of the kink angle α for all three hypotheses under consideration: tau (*solid line*), charm (*dashed line*), and hadronic interactions (*dotted line*). Short vertical lines indicate the values for ν_τ candidate events from Table V.

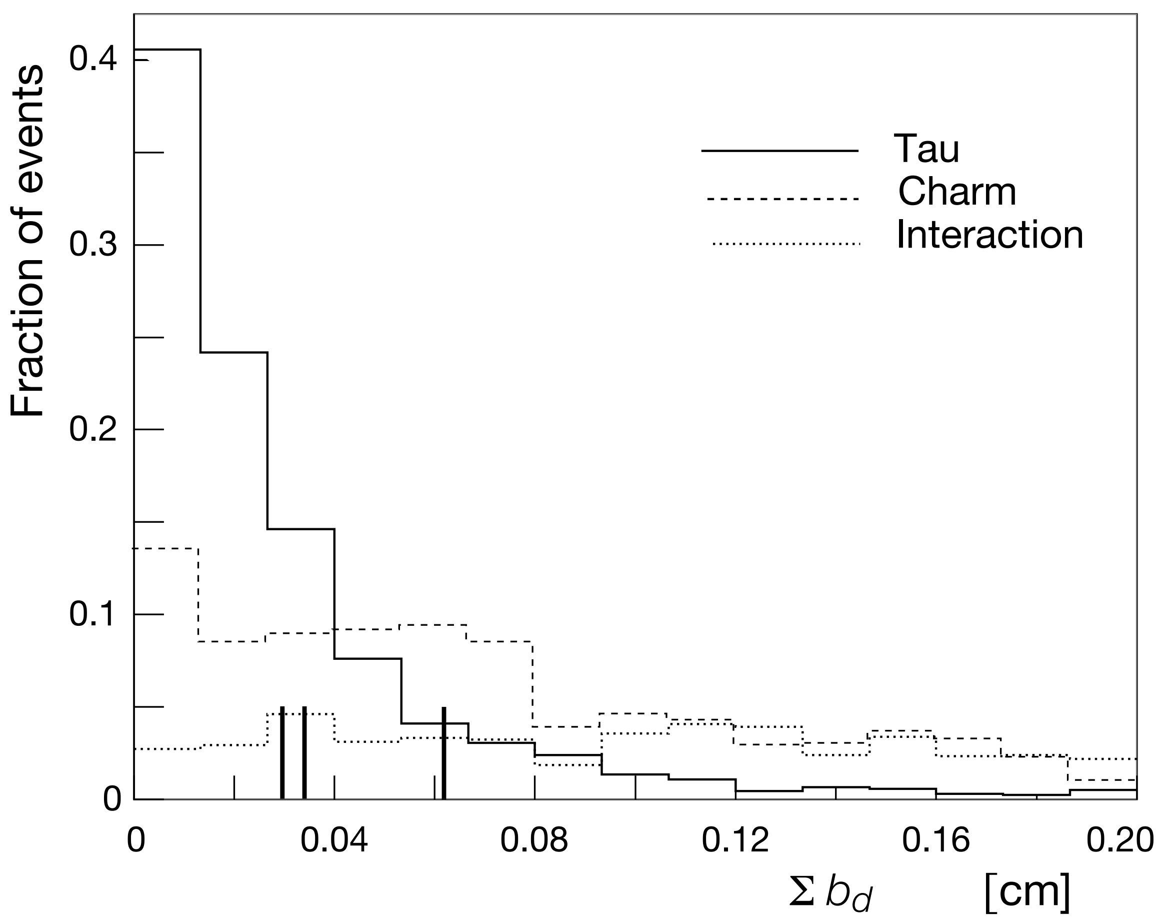

FIG. 14: An example of simulated distributions used as input to the event probability calculation within the multivariate method as applied to three-prong decays. Shown are distributions of $\sum b_d$, the sum of daughter-track impact parameters for all three hypotheses under consideration: tau (*solid line*), charm (*dashed line*), and hadronic interactions (*dotted line*). Short vertical lines indicate the values for ν_τ candidate events from Table V.

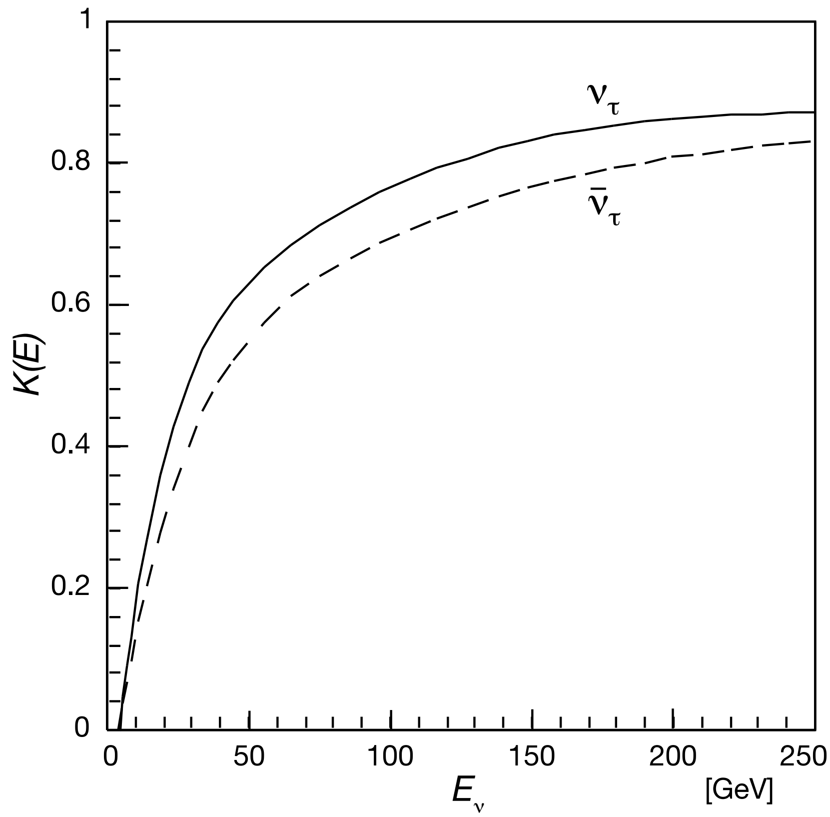

FIG. 15: The tau lepton mass suppresses the ν_τ CC cross section relative to the ν_μ and ν_e cross sections.